Rainwater-driven transport of matter and microbes from phyllosphere to soil in a temperate beech forest

Markus Krüger[1], Karin Potthast[2,3], Beate Michalzik[2,3], Alexander Tischer[2,3,4], Martina Herrmann[1,3,5*]

[1]Institute of Biodiversity, Friedrich Schiller University Jena, Jena, Germany; [2]Department of Soil Science, Friedrich Schiller University Jena, Jena, Germany; [3]German Center for Integrative Biodiversity Research (iDiv) Halle-Jena-Leipzig, Leipzig, Germany, [4]ThüringenForst, Forestry Research and Competence Centre, 99867 Gotha, Germany, [5]Cluster of Excellence Balance of the Microverse, Friedrich Schiller University Jena, Jena, Germany,

*Corresponding author: martina.herrmann@uni-jena.de

Abstract

In forest ecosystems, the transport of organic matter including microbial cells by throughfall and stemflow represents a central linkage between the phyllosphere and soil. However, the extent and taxon-specificity of rainwater-mediated vertical transfer of microorganisms, and its relevance for matter fluxes is sparsely understood. We investigated the rainwater-driven transport of bacteria and its contribution to matter transport along bulk rainfall, throughfall, stemflow and seepage flow paths from the phyllosphere to soil in a temperate deciduous forest. Throughfall-mediated cell fluxes equalled those in seepage below the litter layer, pointing to a substantial above-ground translocation of bacteria. Bacterial cells contributed up to 11 % and 33 % to the exported total organic carbon and total nitrogen, respectively. Bacteria affiliated with *Pseudomonadaceae*, *Oxalobacteraceae*, *Hymenobacteraceae*, and *Sphingomonadaceae* were differentially transmitted from the canopy and enriched in throughfall and stemflow. 117 Amplicon Sequence Variants (ASVs) (1.7 %) occurred in all rainwater flow paths, suggesting a vertical connectivity from the phyllosphere through the soil that allows the continuous import, proliferation, and mobilization of selected bacterial taxa. The genetic potential of the transported bacterial communities was strongly linked to organic matter degradation particularly of carbohydrates and proteins. Our findings extend our understanding of rainwater-mediated vertical matter transport in forest ecosystems and highlight the contribution of microbial cells to this transport especially in above-ground compartments. Strong shifts in community composition and abundance of the transported taxa between throughfall, stemflow and soil seepage are linked to differences in source communities but may also point to different mechanisms of cell detachment across compartments.

37 **Graphical abstract**

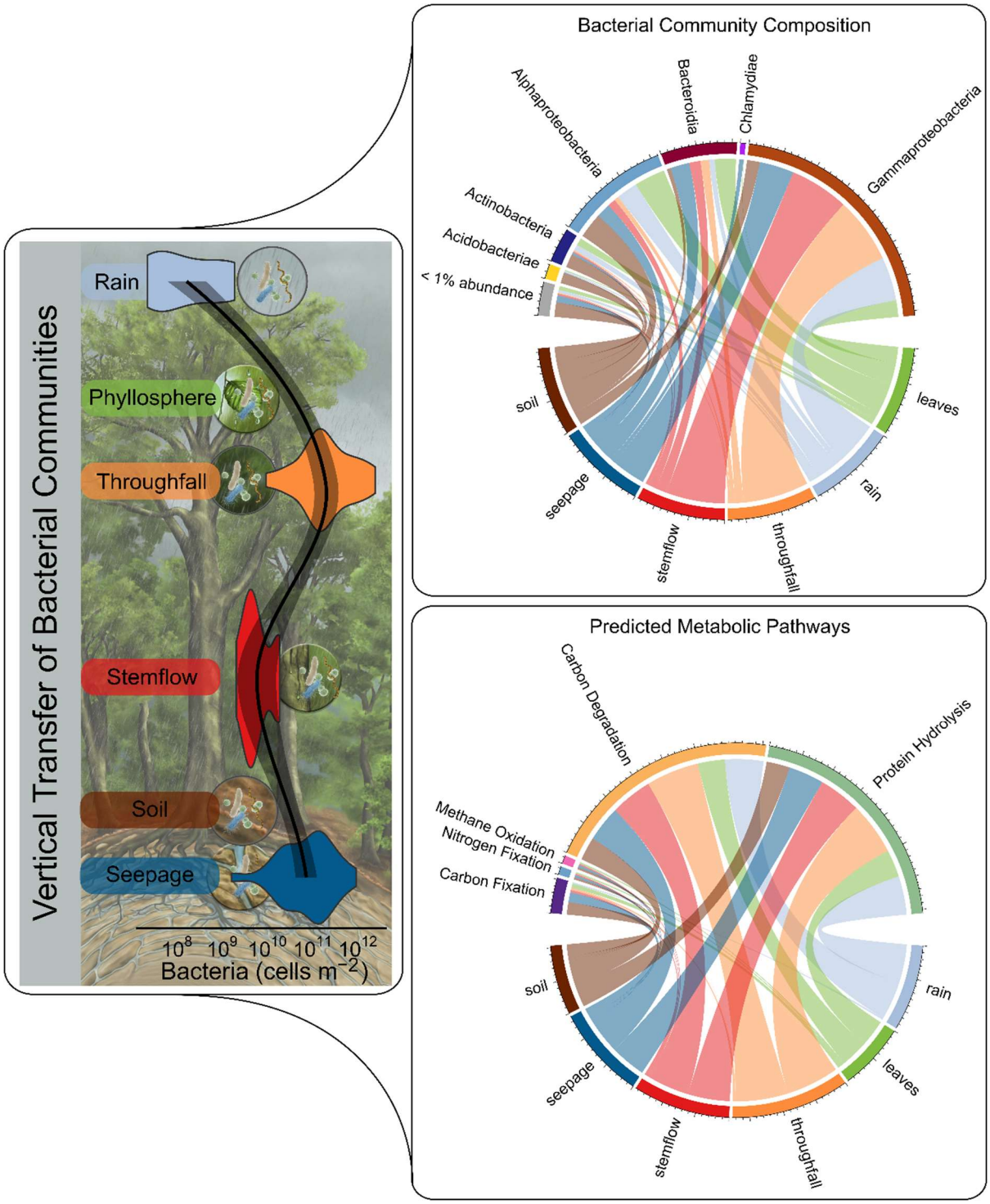

38

39

1. Introduction

Rainwater represents an important carrier of various particles including organic matter and microorganisms across long distances (Hu et al., 2018). Such wet deposition may harbor tens of millions of bacteria m^{-2} d^{-1} (Reche et al., 2018) and other microorganisms such as archaea, fungi and protists (Després et al., 2012; Sánchez-Parra et al., 2021), and thus plays a crucial role in microbial dispersal within ecosystems. Microbes from atmospheric sources may contribute directly to the microbiome of the plant phyllosphere (Ponette-González et al., 2020), which exhibits a global surface area of 6.4 x 10^8 km^2 as microbial habitat (Vorholt, 2012). During rain events, huge amounts of rainwater can pass the forest canopy and emerge as throughfall and stemflow water fluxes (Levia et al., 2011). Throughfall represents that part of precipitation which falls through the canopy, partially along leaf surfaces, while stemflow is defined as the flow path of rainwater which runs down the stem (Sadeghi et al., 2020). In temperate forests, both water flow paths can transport a substantial amount of organic matter ranging between 0.2 – 200 kg C ha^{-1} y^{-1} (Ponette-González et al., 2020; Van Stan et al., 2017) and bacteria in the range of 1.5 x 10^{16} cells ha^{-1} yr^{-1} (Bittar et al., 2018). As consequence, the forest canopy may act as a considerable source of microorganisms, influencing the bacterial composition of rainwater as it is transported down to the forest floor (Sadeghi et al., 2020; Van Stan et al., 2017). A certain proportion of this rainwater further percolates through the soil as seepage, containing mobile organic matter including microorganisms (Dibbern et al., 2014; Krüger et al. 2021; Herrmann et al., 2023; Zhang et al., 2018), resulting in continued microbial transport to subsoils and ultimately to the groundwater (Friesen, 2020).

In the phyllosphere, bacteria perform a variety of matter transformation processes such as carbon- and nitrogen fixation, nitrification and methanol oxidation (Andrews and Harris, 2000; Guerrieri et al., 2020, 2024) . Methanotrophic bacteria such as *Methylomonas* and *Methylobacter, Flavobacterium* and *Novosphingobium* are common members of the microbiome on tree leaf and bark surfaces (Iguchi et al., 2015; Jeffrey et al., 2021). In addition, microbial extracellular enzymes which degrade hydrocarbons and secondary plant

metabolites can be exported from the phyllosphere by throughfall and stemflow (Mori et al., 2019), contributing to exoenzymatic matter degradation in the soil. In contrast to litter fall in autumn, which acts as a periodic mass transfer of organic matter, microorganisms, and their degradation capacity to the forest floor, throughfall and stemflow represent season-independent, high-frequency episodic flow events from the phyllosphere, ensuring connectivity between above-ground and below-ground compartments throughout the year.

Assuming a certain fraction of the microbial cells remains viable during transport, rainwater delivers air- and phyllosphere-derived bacteria which constitute an essential source of new genetic material and functional potential to the sink communities. In fact, previous work demonstrated that some bacteria are selectively washed off from leaves and stems and get enriched along the water flow paths (Guerrieri et al., 2020). Stemflow creates funneling of water along with matter and microbes which are rapidly transported along roots into the soil (Carlyle-Moses et al., 2020; Tischer et al., 2020). In addition, rainwater provides fresh particulate and biolabile dissolved carbon and nitrogen to the forest floor (Michalzik et al., 2001; Van Stan and Stubbins, 2018), which can affect soil nutrient pools (Van Stan et al., 2017) and soil microbial activity (Deng et al., 2017).

Previous studies investigated the microbial diversity and mass fluxes associated with aerosol particles (Després et al., 2012), tree phyllosphere, throughfall and stemflow (Van Stan et al., 2020). However, research is scarce on the quantity and structure of microbial communities transported by rainwater, throughfall, and stemflow, and which fraction of the transported matter originates from microbial cells and their functional potential across different compartments including soil seepage. Seepage-mediated transport of microbes through soils was previously studied at the Hainich Critical Zone Exploratory using lysimeters installed in a beech forest (Krüger et al., 2021; Herrmann et al., 2023). In this study, we used zero tension lysimeters along with bulk rainwater, throughfall and stemflow collectors (Levia et al., 2023; Potthast et al., 2017) to investigate the abundance and community composition of bacterial communities along the flow path from the phyllosphere to soil seepage, along with an

estimation of their functional potential and contributions to matter fluxes. We aimed to (1) estimate bacterial fluxes and contributions to carbon and nitrogen transport in throughfall, stemflow and seepage, comparing an early and late growing season rain event; (2) characterize the bacterial composition of the respective compartments and their predicted functional potential, and (3) assess core and shared communities for each intersection of neighboring compartments to provide insights into the fraction of bacterial communities that can be mobilized along the vertical flow path.

2. Materials and methods

2.1 Study site and sampling procedure

Sampling was conducted in spring and autumn on a managed deciduous temperate forest plot (N51°06'56.5' E10°24'45.2) and on an open area site (N51°07'63.5' E10°23'68.2') in the Hainich-Dün area comprising the Hainich Critical Zone Exploratory, Germany (**Figure 1**A). Forest stands are dominated by European beech (*Fagus sylvatica* L.) with minor admixtures of sycamore maple (*Acer pseudoplatanus* L.) and ash (*Fraxinus excelsior* L.), a common forest composition in the Hainich-Dün area. A nearby, extensively managed grassland site (open area) was used for measurements of bulk precipitation (rainwater). The climate is characterized by annual precipitation of 600 mm and mean air temperature of 9°C (Potthast et al., 2017).

Ten throughfall and four rainwater collectors with a sampling area of 314 cm^2 at approximately 1.2 m height were deployed at a forest and an open area plot 2 km apart, respectively (**Figure 1**B). Stemflow collars were installed at two tree individuals of each *F. sylvatica* and *A. pseudoplatanus* at 1.3 m height with a basal area in breast height between 346 to 740 cm^2. Rainwater, throughfall and stemflow plastic containers were cleaned and surface-disinfected with H_2O_2 prior to exposure and were placed in the field 1 to 2 days before two major rain events in May and September 2020, respectively. All three collector types were equipped with a 2 mm PE mash to avoid the introduction of large particles or insects during the collection period. Seepage was obtained from 16 zero-tension lysimeters with an area of 284 cm^2 accessing soil leachate which percolated the soil through the litter, and the upper 4 cm, 16 cm and 30 cm (Krüger et al., 2021). Details on lysimeter properties and installation were described by Potthast et al., 2017. Residual solution from the lysimeters was emptied before the rain events to obtain only freshly percolated soil leachate. Throughfall, stemflow and seepage solutions at the forest site and bulk rainwater at the pasture site were sampled on 13th May 2020 and 28th September 2020 after rain events of 12 and 19 mm, respectively (**Figure 1**C). Triplicate leaf samples of the phyllosphere from two individuals of *F. sylvatica* and *A.*

128 *pseudoplatanus* at low canopy height of 4 to 5 m were clipped off with ethanol cleaned scissors
129 and stored in autoclaved plastic container after each rain event. In addition, soil samples as
130 reference to the mobilized microbial communities were collected in triplicates close to the
131 lysimeters at 0 to 4 cm, 4 to 16 cm and 16 to 30 cm depths in May 2020. All samples were
132 stored in cooling boxes at approximately 8°C during transport and were immediately
133 processed at the laboratory within 2 h. Rainwater, throughfall, stemflow, and seepage samples
134 were weighed to determine the volume and 10 to 100 ml was used for determination of pH,
135 electrical conductivity, carbon, nitrogen, and elemental analysis. For molecular analyses,
136 water samples were filtered through 0.2 µm polyethersulfone membrane filters (Supor, Pall
137 Corporation, USA) and stored at -80°C. Filtrate was stored at -20°C for determination of
138 inorganic nitrogen. Phyllosphere samples in plastic bottles were treated with 1 min of mild
139 sonification in 250 ml NaCl buffer (0.15 M NaCl + 0.1 % Tween 20) to detach microorganisms
140 from leaf surfaces, followed by 20 min shaking at 100 rpm (Herrmann et al., 2021). Resulting
141 suspensions were filtered through 0.2 µm pore size filters and stored at -80°C until further
142 processing. The remaining leaves were dried at 50°C for 1 week to measure the dry weight.
143 Soil samples for molecular analysis were stored at -80°C while those for determination of dry
144 weight and pH were stored at 4°C.

145 **2.2 Physicochemical analyses and calculation of matter fluxes**

146 Rainwater, throughfall, stemflow, and seepage samples were analyzed for total organic
147 carbon (TOC), inorganic carbon (IC) and total nitrogen (TN) as well as dissolved organic
148 carbon (DOC) and total dissolved nitrogen (TDN) concentrations. Analysis involved filtration
149 through <0.45 µm prewashed membrane filters (cellulose acetate, Sartorius, Göttingen,
150 Germany) for dissolved elements and catalytic thermal oxidation and
151 NDIR/chemiluminescence detection of both non-filtrated and filtrated samples using a TOC-
152 VCPN/TNM-1 (Shimadzu, Duisburg, Germany) (Potthast et al., 2017; Visco et al., 2005).
153 Particulate organic carbon (POC) and total particulate nitrogen (TPN) were calculated by
154 subtracting the dissolved fractions from the total concentrations. Inorganic nitrogen (IN),

155 mainly consisting of NH_4^+ and NO_3^- was determined by standard colorimetric approaches
156 (Scheiner, 1974; Seelmeyer, 1954).

157 Carbon (TOC) and nitrogen (TN) fluxes per rain event were calculated from the concentration
158 of the respective parameters from water samples (rainwater, throughfall, stemflow, seepage)
159 multiplied by the respective sample volume and the collector area and were expressed in mg
160 C or N m^{-2}. Stemflow fluxes were calculated for the individual basal area of each tree specimen
161 and scaled up to the tree stand area in ha from both species.

162 Electrical conductivity and pH were determined using a WTW pH / Cond meter (pH Cond 3320
163 with SenTix81 and TetraCond, Weilheim, Germany) (Potthast et al., 2017). The soil water
164 content was determined by drying the samples over 48 h at 105°C. Soil pH was determined
165 from slurries prepared using sterile deionized water (ratio 1:2.5) and measured with a pH glass
166 electrode (Krüger et al., 2021).

167 **2.3 DNA extraction, quantitative PCR, and amplicon sequencing**

168 Microbial biomass from a filter half (leaves, rainwater, throughfall, stemflow, seepage) and
169 from 0.25 g of soil of each sample were extracted using the DNeasy PowerSoil kit (Qiagen,
170 Germany) following the manufacturer's protocol and stored at -20°C. Bacterial and archaeal
171 16S rRNA gene abundances were quantified with a CFX96 real-time PCR thermocycler (Bio-
172 Rad, USA) using primer pair Bakt_0341F/Bakt_799R (Chelius and Triplett, 2001; Klindworth
173 et al., 2013) which discriminates against chloroplast-derived 16S rRNA genes, and
174 Arch806F/Arch958R (DeLong, 1992; Takai and Horikoshi, 2000), respectively. Details on PCR
175 and cycling conditions are described elsewhere (Herrmann et al., 2021, 2012). Plasmids
176 containing cloned bacterial and archaeal 16S rRNA gene fragments were used to construct
177 qPCR standards, which were linear across the concentration range of 50 to 5 $x10^8$ copies per
178 reaction. Gene abundances in rain, throughfall, stemflow and seepage were calculated as per
179 L, while gene abundance on leaf surfaces and soil was expressed as genes per g of dry
180 weight.

181 Library construction for 16S rRNA gene targeted amplicon sequencing assessing the bacterial
182 community composition across samples was conducted with the same primer pair as for
183 qPCR, targeting the V3-V4 region of the bacterial 16S rRNA gene. Reactions were performed
184 with 1 ng DNA template per sample in 15 µl volume reactions under previously reported
185 conditions (Herrmann et al., 2021). Subsequent steps are described in Krüger et al. (2021),
186 and sequencing was performed on an Illumina MiSeq platform using v3 chemistry.

187 **2.4 Sequence processing and PICRUSt2 analysis**

188 PCR primer sequences were trimmed from raw reads using Cutadapt (Martin, 2011) and reads
189 were further processed with the R package DADA2 1.22.0 following the standard sequence
190 analysis pipeline for 16S rRNA genes (Callahan et al., 2016). Trimmed reads were filtered and
191 denoised using the filterAndTrim function under the following conditions: (truncLen = c(270,
192 240), maxEE = c(2,3), truncQ = 2, maxN = 0). The filtered reads of each sample were
193 dereplicated, Amplicon Sequencing Variants (ASVs) were deduced for forward and reverse
194 reads separately, and then the forward and reverse reads were merged at overlapping
195 positions. Chimeric sequences were removed and taxonomic assignment of amplicon
196 sequence variants (ASV) was performed using the SILVA taxonomy reference database
197 release version 138 (Quast et al., 2013). ASV sequences were extracted and aligned using
198 DECIPHER (Wright, 2020, 2016), and a phylogenetic tree was constructed using phangorn
199 (Schliep, 2011). In depth analysis of the bacterial community was performed in R using the
200 packages phyloseq (McMurdie and Holmes, 2013), vegan (Oksanen et al., 2008) and
201 tidyverse (Wickham et al., 2019) and their dependencies. Non-bacterial sequences assigned
202 to chloroplasts, mitochondria, eukaryotes, and archaea were excluded from further analysis,
203 resulting in 15659 unique ASVs and a median of 20,464 reads per sample. One seepage
204 sample was excluded from analysis due to very low amounts of sequencing reads per sample.
205 Normalization was done by rarefying all reads from each sample using the phyloseq function
206 rarefy_even_depth at a minimum of 4426 sequencing reads per sample. Subsequently, ASVs

207 with only 1 read were excluded from analysis. Shannon and Chao alpha diversity indexes
208 were calculated using the estimate_richness function in phyloseq.

209 2.5 Prediction of microbial functions

210 To approximate the functional potential of the microbial communities across the different
211 compartments, PICRUSt2 (Phylogenetic Investigation of Communities by Reconstruction of
212 Unobserved States) analysis was applied to predict microbial functions based on the obtained
213 amplicon sequencing data using v2.3.0 beta following the standard procedure for 16S rRNA
214 (Douglas et al., 2020). ASV sequences were first aligned and placed into a reference tree and
215 ASVs were corrected for multiple 16S rRNA genes by the 16S rRNA operon number of closely
216 related representatives. Gene families for each ASV were predicted based on KEGG orthologs
217 (KO) as identifiers for metabolic pathways (Kanehisa et al., 2023). The PICRUSt2 output of
218 7,523 KOs was subset for KO abundance of enzymes involved in the following pathways:
219 carbon fixation, nitrogen fixation, methane oxidation, carbon degradation and protein
220 hydrolysis. Metagenomic predictions of the selected pathways were based on the relative
221 abundance of the KO IDs across each sample. To assess the proportion of the bacterial
222 community associated with the selected metabolic functions across samples, we used the
223 relative abundance of each ASV from amplicon sequencing data for which a corresponding
224 KO was predicted.

225 2.6 Determination of absolute cell abundances and cell fluxes

226 Studies have shown that combining amplicon sequencing of marker genes and qPCR can be
227 used as an accurate method to infer cell numbers similar to direct cell determination by flow
228 cytometry (Bittar et al., 2018) and to enhance bacterial community profiling (Jian et al., 2020;
229 Lou et al., 2018). The quantity of exported cells was calculated using the 16S rRNA qPCR-
230 based gene abundances per liter and the amplicon sequencing reads on family-level. To
231 account for diverging operon numbers of the 16S rRNA gene across the 303 observed
232 bacterial families, gene abundances were corrected using the number of operons of the
233 respective family-level taxa obtained from the ribosomal RNA operon database

234 (https://rrndb.umms.med.umich.edu/) (Stoddard et al., 2015). The estimated absolute cell
235 count per liter for each sample of rainwater, throughfall, stemflow and seepage was
236 determined based on the relative read abundance from each taxon multiplied by the total 16S
237 rRNA gene abundance and divided by the family-specific operon numbers. Bacterial cell fluxes
238 per m^{-2} were calculated as described for TOC and TN using the estimated absolute cell
239 abundance per total sample volume and collector area for each sample from the two sampling
240 time points.

241 **2.7 Estimation of bacterial contributions to TOC and TN**

242 The fraction of bacterial cell carbon and nitrogen contributing to TOC and TN in rainwater,
243 throughfall, stemflow and seepage was estimated as previously described (Herrmann et al.,
244 2023; Krüger et al., 2021). Briefly, a mean carbon content of 39 fg per cell and mean nitrogen
245 content of 12 fg per cell was assumed as estimated under carbon-limited and nitrogen-limited
246 conditions (Vrede et al., 2002), respectively. The contribution of bacterial cell carbon and
247 nitrogen to TOC and TN, respectively, was estimated by first multiplying the operon number
248 corrected absolute bacterial abundances as well as the TOC/ TN content per liter by the
249 sample volume. The estimated number of bacterial cells was multiplied by the assumed
250 carbon and nitrogen content per cell. The resulting estimates of microbial cell carbon and
251 nitrogen were then set in relation to the total organic carbon (TOC) and total nitrogen (TN) in
252 the corresponding samples to estimate the bacterial contribution.

253 **2.8 Statistical analysis**

254 All statistical tests were performed using R version 4.12 (R Core Team, 2020) unless
255 otherwise described. Normal distribution of gene abundances and element fluxes were tested
256 with Shapiro-Wilk test. Non-parametric Kruskal-Wallis rank sum test and Dunn's multiple
257 comparison post-hoc test with R package FSA (Ogle et al., 2020) was used to test data for
258 significant differences between the sample types. To assess the contributing factors
259 accounting for the similarity/ dissimilarity of the bacterial community, a Permutational
260 Multivariate Analysis of Variance Using Distance Matrices (PERMANOVA) was conducted

261 using a Bray-Curtis distance matrix and the adonis2 function with 9999 permutations in R
262 package vegan (Oksanen et al., 2008). Nonmetric multidimensional scaling using Bray-Curtis
263 distance matrix was performed to test dissimilarity of the bacterial community between the
264 sample types, the growing seasons and the tree species. To visualize the distribution patterns
265 of abundant bacterial families across different rainwater flow paths and significant
266 environmental factors, a redundancy analysis (RDA) was performed using the decostand
267 function in vegan and Hellinger method for data standardization.

268 The significance of the observed differentiation was tested with ANalysis Of SIMilarity
269 (ANOSIM) using the anosim2 function from vegan. Correlations between microbial gene
270 abundance, TOC, TN and the sample volumes were assessed and visualized using ggpubr
271 (Kassambara, 2023). Relationships between the absolute abundance of the most abundant
272 17 bacterial families and the matter content of water solution samples were determined by
273 pairwise correlation using Spearman's rank coefficient and visualization using
274 ComplexHeatmap (Gu et al., 2016) and its dependencies. The number of shared ASV across
275 the water solution samples was assessed using packages phyloseq (McMurdie and Holmes,
276 2013), MicrobiotaProcess (Xu et al., 2023) and VennDiagram (Chen and Boutros, 2011). The
277 prevalence of dominant ASV representing the core microbiome across the samples was
278 determined using the metagMisc package including phyloseq, vegan, ALDEx2 (Fernandes et
279 al., 2013), metagenomeSeq (Paulson et al., 2013) and DESeq2 (Love et al., 2014). The
280 shared core microbiome of leaf, rain, throughfall and stemflow was assessed by filtering ASV
281 which were present in at least 70 % of the samples using the function
282 phyloseq_filter_prevalence from metagMisc. The sequences of core AVSs from leaf, rain,
283 throughfall and stemflow samples were extracted and placed in a phylogenetic tree using
284 ggtree (Xu et al., 2022). Lastly, the relative abundances of those ASV during both growing
285 seasons were plotted next to the tree as described in (Rolando et al., 2022).

286 The differential abundance of abundant ASV between phyllosphere and canopy-derived flow
287 paths was assessed using the package DESeq2. Unrarefied sequence reads with > 1

sequence across all samples were subset for leaf, throughfall and stemflow sample types. The phyloseq object was converted to a DESeq2 data file and the ASV table was transformed using the median ratio method for differential abundance analysis. In addition, we used the microbiomeMarker package (Cao et al., 2022) to investigate the bacterial community for biomarker ASV on genus level. Linear discriminant analysis (LDA) Effect Size (LEFSe) was performed across all samples using CPM normalization method with a *p* value of 0.05 and LDA cutoff of 4.

295 # 3. Results

296 ## 3.1 Carbon and nitrogen fluxes across compartments

297 The export of total organic carbon (TOC) ranged from 1.4 mg C m^{-2} in stemflow to 1,600 mg
298 C m^{-2} in seepage right below the litter layer and was significantly different between sample
299 types ($p < 0.001$) (**Figure 2**A). Inorganic carbon (IC) fluxes were on average 2 to 4 times lower
300 across all sample types (**Figure S 1**). Total nitrogen (TN) flux varied from as low as 0.1 mg N
301 m^{-2} in stemflow to a maximum of 1,405 mg N m^{-2} in seepage collected after percolation
302 through the upper 16 cm of the soil profile (**Figure 2**A). C:N ratios showed significantly higher
303 values in throughfall and stemflow ($p < 0.001$) compared to rainwater and seepage (**Figure S**
304 **1**). Ammonium flux decreased from rainwater, throughfall and stemflow to the seepage flow
305 path while fluxes of nitrate were highest in seepage (**Figure S 1**).

306 ## 3.2 Microbial gene abundances, estimated cell fluxes, and contributions to C
307 ## and N transport across compartments

308 Bacterial 16S rRNA gene abundances (**Figure S 2**A) differed significantly between the
309 different sample types ($p < 0.001$) and were highest in throughfall and stemflow. Rainwater
310 exhibited on average three orders of magnitude lower gene abundances. In seepage, bacterial
311 16S rRNA gene abundances decreased with increasing collection depth from below the litter
312 layer down to 30 cm soil depth. Archaeal 16S rRNA gene abundances were consistently two
313 to three orders of magnitude lower than bacterial 16S rRNA gene abundances and exhibited
314 an opposing depth-dependent trend in seepage.

315 We further estimated bacterial cell abundances based on qPCR data and amplicon
316 sequencing data, applying family-level corrections for multiple 16S rRNA gene operons per
317 cell (**Table S 1**). Estimated bacterial abundances on leaf surfaces ranged from 1.4 x 10^5 to 5.4
318 x 10^8 cells g^{-1} dry leaf material while soil bacterial abundances ranged from 9.6 x 10^8 to 7.8 x
319 10^9 cells g^{-1} dry soil. In rainwater, estimated bacterial cell abundance ranged from 1.2 x 10^6 to
320 1.6 x 10^8 cells L^{-1} while throughfall and stemflow cell abundances were about 100 times

321 higher, ranging from 5.8 x 10^8 to 3.1 x 10^{11} cells L^{-1} and 7.9 x 10^9 to 2.3 x 10^{11} cells L^{-1},
322 respectively. Seepage bacterial abundance ranged from 3.8 x 10^8 to 3.9 x 10^{10} cells L^{-1} with
323 a decreasing trend with soil depth ($p < 0.01$). Based on estimated cell abundances, we also
324 determined the flux of bacterial cells transported by rain, throughfall, stemflow and seepage
325 of both sampling events. Across all samples and the two sampling time points, cell fluxes
326 ranged from lowest values in rainwater with 2.3 x 10^7 cells m^{-2}, 9.3 x 10^{11} cells m^{-2} by litter
327 seepage to highest export of 2.8 x 10^{12} cells m^{-2} per event by throughfall with significant
328 differences between sample types ($p < 0.001$) (**Figure 2**A). On average, cell fluxes via
329 throughfall and seepage litter were three orders of magnitude higher than in rainwater.
330 Seepage-mediated cell fluxes of seepage collected below 4 cm soil depth were one order of
331 magnitude lower than in throughfall. No differences in estimated cell fluxes were observed
332 between early and late growing season for a given sample type.

333 The transported amount of TOC and TN by rainwater, throughfall, stemflow and seepage were
334 positively correlated with the estimated total bacterial cell abundance per rain event across all
335 sample types and sampling months ($p < 0.05$) (**Figure 2**B), underlining the strong relationship
336 between microbial transport dynamics and matter transport. Estimation of the bacterial
337 contribution to matter transport indicated a significant bacterial contribution across the different
338 water flow pathways ($p < 0.001$) with bacterial cells contributing between 0.006 % of TOC and
339 0.007 % TN in rainwater, and up to 11.3 % TOC and 33.6 % TN in throughfall (**Figure 2**A).

340 **3.3 Bacterial community composition from phyllosphere to soil**

341 The ASV richness and alpha diversity (Shannon index) differed significantly between all
342 sample types (Kruskal-Wallis, $p < 0.001$) (**Figure 3**A). The highest number of different
343 bacterial taxa was observed in seepage, followed by stemflow, soil, leaf surface and
344 throughfall samples, while rainwater samples were the least diverse. Leaf, seepage, and soil
345 communities were on average more diverse than communities from rain, throughfall and
346 stemflow samples ($p < 0.05$). Alpha diversity and species richness of throughfall and stemflow

347 communities were lower during early growing season compared to late growing season ($p <$
348 0.05) while this effect was not observed for the other sample types.

349 Beta diversity analysis of bacterial communities revealed a clear differentiation based on the
350 sampled compartment (ANOSIM, $R^2 = 0.52$, $p < 0.001$) with phyllosphere, seepage and soil
351 communities being distinct, while rainwater, throughfall and stemflow communities appeared
352 very variable and were not clearly separated (**Figure 3**B). Sample type was the strongest
353 driver for the community differentiation, accounting for 25.2 % of the total community variation
354 (PERMANOVA, $p < 0.001$) (**Figure 3**B). The sampling month contributed 2.1 % of the
355 variation. Influence of tree species (European beech versus sycamore maple) explained only
356 less than 1 % of the variation and was not included as influencing factor in further analysis.

357 On family-level, 23 bacterial taxa each comprised more than 1 % of the total community
358 (**Figure S 2**B), which exhibited distinct distribution patterns across rain, throughfall, stemflow
359 and seepage (ANOSIM: $R^2 = 0.54$, $p < 0.001$). Gammaproteobacteria, Alphaproteobacteria,
360 Bacteroidia, Actinobacteria and Acidobacteriae accounted for at least 90 % of all sequence
361 reads across all samples (**Figure 3**C). Across rainwater, throughfall and stemflow samples,
362 *Pseudomonadaceae* accounted for a large proportion of between 24 – 42 % together with
363 common plant pathogens such as *Erwiniaceae* and *Yersiniaceae*, particularly during the early
364 growing season. In phyllosphere samples, *Hymenobacteraceae* (32 mean ± 7 % standard
365 deviation) dominated at the late growing season sampling point together with
366 *Sphingomonadaceae* (16 ± 7 %) while *Beijerinckiaceae* (13 ± 6 %) were more abundant at the
367 early growing season. In contrast to rainwater, throughfall and stemflow,
368 Gammaproteobacteria were less abundant in phyllosphere samples and were here mostly
369 represented by *Oxalobacteraceae* (5 ± 3 %) and *Comamonadaceae* (6 ± 4 %) in the early and
370 late growing season samples, respectively. In soil communities, Alphaproteobacteria
371 accounted on average for 24 ± 3 % with *Xanthobacteraceae* being the dominant family (19 ±
372 3 %). Seepage communities were dominated by *Flavobacteriaceae, Oxalobacteraceae* and
373 *Comamonadaceae*.

374 The taxonomic composition derived from estimated cell abundances confirmed the patterns
375 revealed by relative read abundances (**Figure S 2**C). Analysis based on absolute abundance
376 revealed that most of rainwater-derived bacterial families, including *Pseudomonadaceae*,
377 *Yersiniaceae* and *Sphingomonadaceae*, were enriched by two to five orders of magnitude in
378 throughfall and stemflow. In contrast to those communities, the bacteria in seepage depicted
379 a two to three orders of magnitude increase in cell abundance of taxa such as
380 *Xanthobacteraceae*, *Spirosomaceae* and *Diplorickettsiaceae,* which showed also high relative
381 abundances in soil communities.

382 **3.4 Predicted metagenomic functions of bacterial communities**

383 The prediction of the bacterial genetic repertoire for selected biogeochemical transformations
384 unveiled distinct patterns across the sample types (**Figure S 3**, ANOSIM: $R^2 = 0.42$, $p < 0.001$).
385 The predicted relative abundance of KOs showed that most pathways had higher prevalence
386 towards soil and leaf communities except for protein hydrolysis, which was more prevalent in
387 bacteria transported by seepage.

388 The functional metagenomic prediction was based on the presence and absence of functional
389 modules of each pathway (**Figure 4**A). Hydrolytic enzymes showed high relative abundances
390 of methionyl aminopeptidase (0.083 %) and leucyl aminopeptidase (0.062 %) across the
391 samples. Potential for the degradation of carbon sources was also highly prevalent across the
392 samples depicted by beta-N-acetylhexosaminidase (0.046 %), hexosaminidase (0.033 %),
393 beta-glucosidase (0.029 %), chitinase (0.022 %) and alpha-amylase (0.017 %). Potential for
394 carbon fixation was mostly associated with the Calvin–Benson–Bassham pathway,
395 represented by *cbbS* and *cbbL* genes with an average relative abundance of 0.002 % and
396 0.006 %. Nitrogenases as primary enzymes for nitrogen fixation were prevalent in soil (0.0037
397 %), phyllosphere (0.0022 %) and seepage communities (0.0018 %). Methane oxidation was
398 primary related to methanol dehydrogenase (0.0014 %) across all samples, with the highest
399 relative fraction in phyllosphere (0.0037 %) and rainwater communities (0.0024 %).

400 A similar pattern of the functional profiles across the sample types was observed based on
401 relative abundance of bacterial classes for which predicted KO were present (**Figure 4**B). The
402 prevalence of bacteria which showed functional potential differed significantly between the
403 sample types for each pathway ($p < 0.05$). The fraction of bacterial communities showing
404 capability of utilizing enzymes involved in various carbon and protein decomposition
405 processes ranged, on average, from 52 % in throughfall to 75 % in seepage and 60 % in
406 throughfall to 80 % in leaf samples, respectively. Carbon fixation made up by a fraction of 2 %
407 to 13 % of the bacterial community with lowest potential in throughfall and stemflow, and
408 highest potential in seepage samples. Pathways related to biological nitrogen fixation and
409 methane oxidation showed the highest prevalence of 2.5 % and 1.1 %, respectively, in leaf
410 communities, while rain and throughfall communities showed functional potential for both
411 pathways of less than 1 %.

412 **3.5 Connectivity of bacterial communities along the rainwater flow path**

413 Only a small proportion of 1.7 % (117 ASVs of all ASVs) of the bacterial community was shared
414 across all water sample types. The major fraction of 62 % of all ASVs were exclusively present
415 in seepage, while less than 10 % of the total ASVs were only found in either rain, throughfall
416 or stemflow communities (**Figure S 4**). Stemflow communities shared 5.9 % of the ASVs with
417 rainwater, 10.7 % with throughfall, and 6.9 % with seepage.

418 We defined bacterial core taxa based on occurrence in at least 70 % of all samples and tracked
419 the enrichment or decline of single core ASVs from rainwater to phyllosphere and transport by
420 throughfall, stemflow to seepage. Core taxa which constituted a large community fraction on
421 leaves included members of the *Hymenobacteraceae*, *Acetobacteraceae*, *Bejierinckiaceae*
422 and *Sphingomonadaceae*. ASVs affiliated with the genera *Hymenobacter*, *Acidiphilium*,
423 *Methylorubrum* and *Sphingomonas* accounted for up to 1 % relative abundance of the total
424 community on leaves but were less abundant in rainwater. Some ASVs classified as
425 *Sphingomonas* were also observed in throughfall and stemflow (**Figure 5**). Among the
426 phyllosphere community, *Acidiphilium*, *Methylorubrum* and *Sphingomonas* were also

observed in rainwater. In contrast, *Pseudomonadaceae* and *Oxalobacteraceae* including the genera *Pseudomonas* and *Massilia*, respectively, were abundant in rainwater, transferred via throughfall and stemflow and ultimately exported by seepage but were less abundant on leaves.

In addition to the preferential association of core ASVs with a specific sample type, we determined the differential abundance of genus-level taxa which showed either the tendency to stick on leaf surfaces or to be washed off by throughfall and stemflow (**Figure S 5**), indicating their potential as dispersal agents between microbial habitats. Members of *Pseudomonadaceae*, *Yersiniaceae* and *Oxalobacteraceae* were highly enriched in throughfall and stemflow while *Sphingomonadaceae* and *Hymenobacteraceae* showed stronger association with the phyllosphere. Instead, members of *Xanthobacteraceae* and *Flavobacteriaceae* were more enriched in seepage compared to throughfall and stemflow (**Figure S 6**), and *Flavobacteriaceae* and *Sphingomonadaceae* were strongly enriched in seepage compared to soil. LEFSe analysis confirmed the specific association of those bacterial taxa with either the tree phyllosphere or the different mobile fractions along the vertical water flow path (**Figure S 7**).

443 # 4. Discussion

444 Precipitation events transmit a vast number of organic particles, including microbes,
445 representing a major environmental agent connecting the atmosphere with the phyllosphere,
446 pedosphere and lithosphere (Ponette-González et al., 2020; Van Stan et al., 2020). The
447 transported matter and microbial cells can potentially impact microbial communities and
448 nutrient cycling along the water flow path from the plant phyllosphere to soil (Van Stan and
449 Stubbins, 2018; Van Stan et al., 2020). However, the extent of rainwater-driven microbial
450 mobilization within the forest phyllosphere and from bark surfaces, and its contribution to
451 carbon and nitrogen fluxes have so far remained unknown. Here, we assessed the diversity
452 and abundance of bacteria along this flow path, starting from intercepting rain via tree canopy-
453 derived throughfall and stemflow to soil seepage in a temperate forest area at an early and
454 late stage of the growing season.

455 Our results clearly demonstrate that canopy-derived throughfall and stemflow microbial
456 communities are quantitatively important carriers of organic matter to the forest floor,
457 contributing up to 11 and 34 % to total carbon and nitrogen fluxes, respectively. Thus, they
458 play a central role in the throughfall- and stemflow-mediated provision of fresh organic carbon
459 and nitrogen to the forest floor (Van Stan et al., 2021). Throughfall and stemflow obtained in
460 this study from a beech forest during a three-days rain event were highly enriched with bacteria
461 with 10 to 1000 higher estimated cell numbers than previously reported from a subtropical
462 oak-cedar forest (Bittar et al., 2018). Given the fact that throughfall and stemflow samplers
463 were directly sampled at the end of a three-days rain event at overall low ambient
464 temperatures between 0-20°C, we can exclude that massive growth of bacterial cells in the
465 samplers may have led to a strong overestimation of these bacterial loads. Despite on average
466 similar cell concentrations L^{-1} in throughfall and stemflow solutions, stemflow-mediated cell
467 fluxes normalized to tree area were two orders of magnitude lower than in throughfall, which
468 is typically also observed for TOC and TN fluxes when comparing these two water flow paths
469 (Van Stan and Stubbins, 2018). Throughfall cell fluxes were comparable to those from

seepage collected below the litter layer, indicating a substantial above-ground translocation of bacteria to soil.

In contrast to the high estimated proportions of bacterial derived carbon and nitrogen in throughfall and stemflow, bacterial contributions to TOC and TN were three times lower in seepage solutions, matching with previously reported values from the same lysimeters (Krüger et al., 2021) and tension-controlled lysimeters from the same field site (Herrmann et al., 2023). Total estimated cell fluxes were even ten times lower in seepage below 16 cm compared to throughfall. Apparently, a large fraction of the cells mobilized by throughfall and stemflow get retained in the soil, which acts as a strong filter for this above-ground transport. Turnover processes in the soil result in carbon and nitrogen export primarily as dissolved compounds with a lower contribution of mobilized microbial cells. During rain events, throughfall and stemflow mediated inputs might supplement the nutrient pool of the forest litter and soil and could additionally affect microbial nutrient cycling capabilities by introducing active microorganisms with their respective biodegradation capabilities or exoenzymes from upstream communities. Pathway predictions indeed indicated that bacterial communities from throughfall, stemflow and seepage exhibited strong potential for hydrolytic degradation of carbohydrates and proteins. However, since PICRUSt2 only predicts metagenomic functions from marker gene abundance and phylogenetic placement to reference sequences (Douglas et al., 2020), speculations about the full degradation potential need to be treated with caution.

The type of canopy-derived water flow path (throughfall versus stemflow) was the strongest effector for bacterial community similarity/ dissimilarity, suggesting that the composition of the phyllosphere versus bark-associated source communities and potential differences in microbial detachment mechanisms between these two habitats could underlie the observed community differences. Phyllosphere communities were more similar to rain, throughfall and stemflow communities than to seepage and soil, suggesting an exchange of microbes between phyllosphere, throughfall and stemflow in a taxon-specific manner. Rainwater can potentially support the colonization but also the wash-off of epiphytic microbes from leaf

surfaces (Guerrieri et al., 2020). The observed fraction of 10 % of shared taxa between throughfall and stemflow communities suggested that runoff from the canopy exported a basic, selective fraction of bacteria independent of the phyllosphere location, which was further modulated by exchange with the specific colonizers of either leaves or bark (Guerrieri et al., 2020; Teachey et al., 2018). Similarly, Hudson et al. (2023) demonstrated that the bacterial community composition in stemflow was distinct from that found on tree bark. Bark-water interactions during rainfall may lead to the detachment of loosely attached microbes and enable their accumulation further down as major infiltration source in soil (Carlyle-Moses et al., 2020).

Weather conditions and tree species were identified as important factors shaping throughfall bacterial communities in a mediterranean holm oak forest (Guerrieri et al., 2020) and a subtropical Southern live oak forest (Teachey et al., 2018) with Alphaproteobacteria, Gammaproteobacteria and Bacteroidia representing main bacterial classes. Following the above-ground flow path at our study site, *Pseudomonadaceae*, *Erwiniaceae*, *Oxalobacteraceae* and *Sphingobacteriaceae* were introduced into the phyllosphere by rainfall and depicted 10 to 100 times enrichment in relative abundance on leaf surfaces compared to rainwater before being selectively transported by throughfall and stemflow to the soil. Our results further demonstrated a substantial difference in the microbial communities of the above-ground flow paths when comparing an early and late time point of the growing season. During May sampling, *Pseudomonadaceae* accounted on average for over 50 % of the total community in bulk rain, throughfall and stemflow, indicating that at this time point, only a single taxonomic group contributed substantially to matter transport and potential carbon degradation capabilities. *Pseudomonas* species act as common pathogens and epiphytic plant commensals in the phyllosphere (Vorholt, 2012). However, they are also typically observed among microbes attached to plant pollen (Manirajan et al., 2018; Williams, 2013), which can be transmitted by dry deposition (Sánchez-Parra et al., 2021) and rainwater (Cho and Jang, 2014). Higher pollen bioaerosols or pollen deposits derived from the flowering of

524 beech or nearby Norway spruce stands in May might have constituted a large microbial source
525 of pollen-associated *Pseudomonadaceae* in rainwater, throughfall and stemflow (Guidone et
526 al., 2021).

527 The observed distinction of bacterial communities in seepage versus throughfall and stemflow
528 may not only be linked to differences in the bacterial source communities but also to
529 differences in the general bacterial detachment mechanisms between above-ground and
530 below-ground habitats. Preferential, taxon-specific microbial transport through soil by
531 seepage-mediated translocation is mainly attributed to cellular characteristics such as cell
532 size, shape and surface charge (i.e., Zeta potential) (Dibbern et al., 2014; Herrmann et al.,
533 2023; Zhang et al., 2018). In the phyllosphere, the main factor controlling the preferential
534 transfer from leaf surfaces to throughfall might be the strength of attachment to the surface
535 rather than cell size. Members of the *Pseudomonadaceae* can increase local water availability
536 of leaf surfaces by releasing surfactants, allowing proliferation (Koskella, 2020), which might
537 also be a reason for preferential mobilization and detachment of members of this family by
538 throughfall and stemflow. In addition, surfactants may also support the detachment of other
539 leaf-associated microorganisms. Prevalent bacterial epiphytes from the phyllosphere beyond
540 *Pseudomonadaceae* are *Methylobacteriaceae* and *Sphingomonadaceae* (Bashir et al., 2022;
541 Delmotte et al., 2009; Lindow and Brandl, 2003; Vacher et al., 2016; Vorholt, 2012), which
542 were also observed in rainwater at our study site, depicting the connectivity between
543 atmosphere, phyllosphere and pedosphere. Especially *Pseudomonadaceae* could also
544 constitute an important source of extracellular exoenzymes performing hydrolytic degradation,
545 affecting decomposition of soil organic matter (Mori et al., 2019).

546 Despite the high numbers of cells transported by throughfall and stemflow, it remains an open
547 question whether cells remain viable throughout the whole vertical passage, and how many
548 living microbes ultimately reach the soil. The fact that we were able to trace individual ASVs
549 from the phyllosphere to throughfall, stemflow and seepage samples demonstrates that
550 distinct members of the bacterial community at least remained intact during this continuous

passage or were successfully transferred between two neighboring compartments. A seepage study using electron microscopy further indicated that living microbes remained intact during soil passage across 60 cm depth by seepage transmission (Dibbern et al., 2014).

Our results further suggest that multiple taxa were able to colonize and thrive in all of the investigated ecosystem compartments from atmosphere to soil. Establishment and proliferation in the respective compartments probably ensure that the taxa can also be released again from these compartments and be transported again along the flow path. However, with our approach, we cannot distinguish between continuous cross-compartment transport of individual cells or discontinuous transport, resulting from establishment in each compartment, proliferation, and subsequent secondary mobilization of microbial taxa. Consequently, occurrence of the same ASVs across the vertical flow path does not necessarily indicate an uninterrupted flow of individual cells through the system but the ability of certain taxa to be continuously mobilized from one compartment and transported to the other, and to establish stable populations in the respective sink communities, from whereon cells can be mobilized again, resulting in the observed continuity and connectivity of microbial communities and their functional potential.

5. Conclusions

Our study clearly demonstrates that microorganisms transported by rainwater, throughfall, stemflow and seepage contribute substantially to carbon and nitrogen fluxes in a deciduous forest ecosystem. Contributions and cell fluxes were larger in above-ground compared to below-ground compartments, suggesting that a considerable fraction of mobilized cells was retained in the soil and not further transported. Throughfall- and stemflow-mediated flow paths act as substantial carriers of microbial biomass, carbon and nitrogen which might affect soil matter transformation by introducing a fresh source of nutrients but also new genetic variability to the respective microbial sink communities along the flow path. In contrast to periodic cell and nutrient inputs via litter fall, the throughfall- and stemflow-mediated vertical microbial transport to the forest floor throughout the year, acting as central connection between

phyllosphere and forest floor in terms of carbon and nitrogen inputs but also as contribution to the functional diversity of soil microbiomes. Our results further expand a previously observed taxon-specificity in seepage-mediated microbial mobilization in soil to throughfall and stemflow, presumably along with different mechanisms of microbial detachment across these flow paths.

Data availability

Raw sequence files were deposited at the European Nucleotide Sequence Archive with project number PRJEB92466 under accessions ERS25231161 to ERS25231303.

Acknowledgements

We thank Falko Gutmann, Stefan Riedel and Linda Gorniak for support of field and laboratory work, and Martin Stephan from the Otto Schott Institute for Materials Research at Friedrich Schiller University Jena for producing customized soil lysimeters. We are further grateful for the background graphics provided by Clemens Schulze.

Funding

This study was part of the Collaborative Research Centre 1076 AquaDiva (CRC AquaDiva) of the Friedrich Schiller University Jena, funded by the Deutsche Forschungsgemeinschaft under project number 218627073. The infrastructure for MiSeq Illumina sequencing was financially supported by the Thüringer Ministerium für Wirtschaft, Wissenschaft und Digitale Gesellschaft (TMWWDG project 2016 FGI 0024 “BIODIV”).

Author contributions: CRediT

Markus Krüger: Conceptualization, Formal analysis, Investigation, Methodology, Visualization, Writing – original draft, Writing – review and editing. Karin Potthast: Conceptualization, Methodology, Writing – review and editing. Beate Michalzik: Conceptualization, Writing – review and editing. Alexander Tischer: Conceptualization, Methodology, Writing – review and editing. Martina Herrmann: Funding acquisition, Conceptualization, Sample processing, Writing – review and editing.

Declaration of competing interest

The authors declare that the work of this study was achieved without financial or personal conflict of interest.

References

Andrews, J.H., Harris, R.F., 2000. The ecology and biogeography of microorganisms on plant surfaces. Annu. Rev. Phytopathol. 38, 145-180. https://doi.org/10.1146/annurev.phyto.38.1.145

Bashir, I., War, A.F., Rafiq, I., Reshi, Z.A., Rashid, I., Shouche, Y.S., 2022. Phyllosphere microbiome: Diversity and functions. Microbiol. Res. 254, (126888). https://doi.org/10.1016/j.micres.2021.126888

Bittar, T.B., Pound, P., Whitetree, A., Moore, L.D., Van Stan, J.T., 2018. Estimation of Throughfall and Stemflow Bacterial Flux in a Subtropical Oak-Cedar Forest. Geophys. Res. Lett. 45, 1410–1418. https://doi.org/10.1002/2017GL075827

Callahan, B.J., McMurdie, P.J., Rosen, M.J., Han, A.W., Johnson, A.J.A., Holmes, S.P., 2016. DADA2: High-resolution sample inference from Illumina amplicon data. Nat. Methods 13, 581–583. https://doi.org/10.1038/nmeth.3869

Cao, Y., Dong, Q., Wang, D., Zhang, P., Liu, Y., Niu, C., 2022. microbiomeMarker: an R/Bioconductor package for microbiome marker identification and visualization. Bioinformatics 38, 4027–4029. https://doi.org/10.1093/bioinformatics/btac438

Carlyle-Moses, D.E., Iida, S., Germer, S., Llorens, P., Michalzik, B., Nanko, K., Tanaka, T., Tischer, A., Levia, D.F., 2020. What We Know About Stemflow's Infiltration Area. Front. For. Glob. Chang. 3, (532805). https://doi.org/10.3389/ffgc.2020.577247

Chelius, M.K., Triplett, E.W., 2001. The diversity of archaea and bacteria in association with the roots of Zea mays L. Microb. Ecol. 41, 252–263. https://doi.org/10.1007/s002480000087

Chen, H., Boutros, P.C., 2011. VennDiagram: A package for the generation of highly-customizable Venn and Euler diagrams in R. BMC Bioinformatics 12, 35. https://doi.org/10.1186/1471-2105-12-35

Cho, B.C., Jang, G. Il, 2014. Active and diverse rainwater bacteria collected at an inland site in spring and summer 2011. Atmos. Environ. 94, 409–416. https://doi.org/10.1016/j.atmosenv.2014.05.048

Delmotte, N., Knief, C., Chaffron, S., Innerebner, G., Roschitzki, B., Schlapbach, R., Von Mering, C., Vorholt, J.A., 2009. Community proteogenomics reveals insights into the physiology of phyllosphere bacteria. Proc. Natl. Acad. Sci. U. S. A. 106, 16428–16433. https://doi.org/10.1073/pnas.0905240106

DeLong, E.F., 1992. Archaea in coastal marine environments. Proc. Natl. Acad. Sci. 89, 5685–5689. https://doi.org/10.1073/pnas.89.12.5685

Deng, Q., Hui, D., Chu, G., Han, X., Zhang, Q., 2017. Rain-induced changes in soil CO2 flux and microbial community composition in a tropical forest of China. Sci. Rep. 7, 5539. https://doi.org/10.1038/s41598-017-06345-2

Després, V.R., Alex Huffman, J., Burrows, S.M., Hoose, C., Safatov, A.S., Buryak, G., Fröhlich-Nowoisky, J., Elbert, W., Andreae, M.O., Pöschl, U., Jaenicke, R., 2012. Primary biological aerosol particles in the atmosphere: A review. Tellus, Ser. B Chem. 64, (15598). Phys. Meteorol. https://doi.org/10.3402/tellusb.v64i0.15598

Dibbern, D., Schmalwasser, A., Lueders, T., Totsche, K.U., 2014. Selective transport of plant root-associated bacterial populations in agricultural soils upon snowmelt. Soil Biol. Biochem. 69, 187–196. https://doi.org/10.1016/j.soilbio.2013.10.040

652 Douglas, G.M., Maffei, V.J., Zaneveld, J.R., Yurgel, S.N., Brown, J.R., Taylor, C.M.,
653 Huttenhower, C., Langille, M.G.I., 2020. PICRUSt2 for prediction of metagenome
654 functions. Nat. Biotechnol. 38, 685-688. https://doi.org/10.1038/s41587-020-0548-6

655 Fernandes, A.D., Macklaim, J.M., Linn, T.G., Reid, G., Gloor, G.B., 2013. ANOVA-Like
656 Differential Expression (ALDEx) Analysis for Mixed Population RNA-Seq. PLoS One 8,
657 e67019. https://doi.org/10.1371/journal.pone.0067019

658 Friesen, J., 2020. Flow pathways of throughfall and stemflow through the subsurface, in:
659 Precipitation Partitioning by Vegetation: A Global Synthesis. Springer International
660 Publishing, pp. 214–227. https://doi.org/10.1007/978-3-030-29702-2_13

661 Gu, Z., Eils, R., Schlesner, M., 2016. Complex heatmaps reveal patterns and correlations in
662 multidimensional genomic data. Bioinformatics 32, 2847–2849.
663 https://doi.org/10.1093/bioinformatics/btw313

664 Guerrieri, R., Cáliz, J., Mattana, S., Barceló, A., Candela, M., Elustondo, D., Fortmann, H.,
665 Hellsten, S., Koenig, N., Lindroos, A.J., Matteucci, G., Merilä, P., Michalski, G., Nicolas,
666 M., Thimonier, A., Turroni, S., Vanguelova, E., Verstraeten, A., Waldner, P., Watanabe,
667 M., Casamayor, E.O., Peñuelas, J., Mencuccini, M., 2024. Substantial contribution of
668 tree canopy nitrifiers to nitrogen fluxes in European forests. Nat. Geosci. 17, 130–136.
669 https://doi.org/10.1038/s41561-023-01364-3

670 Guerrieri, R., Lecha, L., Mattana, S., Cáliz, J., Casamayor, E.O., Barceló, A., Michalski, G.,
671 Peñuelas, J., Avila, A., Mencuccini, M., 2020. Partitioning between atmospheric
672 deposition and canopy microbial nitrification into throughfall nitrate fluxes in a
673 Mediterranean forest. J. Ecol. 108, 626–640. https://doi.org/10.1111/1365-2745.13288

674 Guidone, M., Gordon, D.A., Van Stan, J.T., 2021. Living particulate fluxes in throughfall and
675 stemflow during a pollen event. Biogeochemistry 153, 323–330.
676 https://doi.org/10.1007/s10533-021-00787-7

677 Herrmann, M., Geesink, P., Richter, R., Küsel, K., 2021. Canopy Position Has a Stronger
678 Effect than Tree Species Identity on Phyllosphere Bacterial Diversity in a Floodplain
679 Hardwood Forest. Microb. Ecol. 81, 157–168. https://doi.org/10.1007/s00248-020-
680 01565-y

681 Herrmann, M., Hädrich, A., Küsel, K., 2012. Predominance of thaumarchaeal ammonia
682 oxidizer abundance and transcriptional activity in an acidic fen. Environ. Microbiol. 14,
683 3013–3025. https://doi.org/10.1111/j.1462-2920.2012.02882.x

684 Herrmann, M., Lehmann, K., Totsche, K.U., Küsel, K., 2023. Seepage-mediated export of
685 bacteria from soil is taxon-specific and driven by seasonal infiltration regimes. Soil Biol.
686 Biochem. 187, 109192. https://doi.org/10.1016/J.SOILBIO.2023.109192

687 Hu, W., Niu, H., Murata, K., Wu, Z., Hu, M., Kojima, T., Zhang, D., 2018. Bacteria in
688 atmospheric waters: Detection, characteristics and implications. Atmos. Environ. 179,
689 201-221. https://doi.org/10.1016/j.atmosenv.2018.02.026

690 Hudson, J.E., Levia, D.F., Yoshimura, K.M., Gottel, N.R., Hudson, S.A., Biddle, J.F., 2023.
691 Mapping bark bacteria: initial insights of stemflow-induced changes in bark surface
692 phyla. Microbiol. Spectr. 11, e03562-23. https://doi.org/10.1128/spectrum.03562-23

693 Iguchi, H., Yurimoto, H., Sakai, Y., 2015. Interactions of methylotrophs with plants and other
694 heterotrophic bacteria. Microorganisms. 3, 137-151.
695 https://doi.org/10.3390/microorganisms3020137

696 Jeffrey, L.C., Maher, D.T., Chiri, E., Leung, P.M., Nauer, P.A., Arndt, S.K., Tait, D.R.,
697 Greening, C., Johnston, S.G., 2021. Bark-dwelling methanotrophic bacteria decrease

methane emissions from trees. Nat. Commun. 12, 2127. https://doi.org/10.1038/s41467-021-22333-7

Kanehisa, M., Furumichi, M., Sato, Y., Kawashima, M., Ishiguro-Watanabe, M., 2023. KEGG for taxonomy-based analysis of pathways and genomes. Nucleic Acids Res. 51, 587–592. https://doi.org/10.1093/nar/gkac963

Kassambara, A., 2023. “ggplot2” Based Publication Ready Plots.

Klindworth, A., Pruesse, E., Schweer, T., Peplies, J., Quast, C., Horn, M., Glöckner, F.O., 2013. Evaluation of general 16S ribosomal RNA gene PCR primers for classical and next-generation sequencing-based diversity studies. Nucleic Acids Res. 41, e1. https://doi.org/10.1093/nar/gks808

Koskella, B., 2020. The phyllosphere. Curr. Biol. 30, 1143-1146. https://doi.org/10.1016/j.cub.2020.07.037

Krüger, M., Potthast, K., Michalzik, B., Tischer, A., Küsel, K., Deckner, F.F.K., Herrmann, M., 2021. Drought and rewetting events enhance nitrate leaching and seepage-mediated translocation of microbes from beech forest soils. Soil Biol. Biochem. 154, 108153. https://doi.org/10.1016/j.soilbio.2021.108153

Levia, D., Bischoff, S., Gruselle, M.-C., Näthe, K., Legates, D.R., Lutgen, A.N., Boyer, E.W., Michalzik, B., 2023. Geometric configurations of particulate matter in terrestrial solutions of a temperate beech forest. J. Aerosol Sci. 106196. https://doi.org/10.1016/J.JAEROSCI.2023.106196

Levia, D.F., Keim, R.F., Carlyle-Moses, D.E., Frost, E.E., 2011. Throughfall and Stemflow in Wooded Ecosystems, in: Forest Hydrology and Biogeochemistry. pp. 425–443. https://doi.org/10.1007/978-94-007-1363-5_21

Lindow, S.E., Brandl, M.T., 2003. Microbiology of the Phyllosphere. Appl. Environ. Microbiol. 69, 1875–1883. https://doi.org/10.1128/AEM.69.4.1875

Love, M.I., Huber, W., Anders, S., 2014. Moderated estimation of fold change and dispersion for RNA-seq data with DESeq2. Genome Biol. 15. https://doi.org/10.1186/s13059-014-0550-8

Manirajan, B.A., Maisinger, C., Ratering, S., Rusch, V., Schwiertz, A., Cardinale, M., Schnell, S., 2018. Diversity, specificity, co-occurrence and hub taxa of the bacterial-fungal pollen microbiome. FEMS Microbiol. Ecol. 94, 112. https://doi.org/10.1093/femsec/fiy112

Martin, M., 2011. Cutadapt removes adapter sequences from high-throughput sequencing reads. EMBnet.journal 17, 10. https://doi.org/10.14806/ej.17.1.200

McMurdie, P.J., Holmes, S., 2013. Phyloseq: an R package for reproducible interactive analysis and graphics of microbiome census data. PLoS One 8, e61217. https://doi.org/10.1371/journal.pone.0061217

Michalzik, B., Kalbitz, K., Park, J.H., Solinger, S., Matzner, E., 2001. Fluxes and concentrations of dissolved organic carbon and nitrogen - A synthesis for temperate forests. Biogeochemistry 52, 173–205. https://doi.org/10.1023/A:1006441620810

Mori, T., Wang, S., Zhang, W., Mo, J., 2019. A potential source of soil ecoenzymes: From the phyllosphere to soil via throughfall. Appl. Soil Ecol. 139, 25–28. https://doi.org/10.1016/j.apsoil.2019.02.004

Ogle, D., Wheeler, P., Dinno, A., 2020. FSA: Fisheries Stock Analysis. R package version 0.8.31.

Oksanen, J., Kindt, R., Legendre, P., O’Hara, B., Simpson, G.L., Solymos, P.M., Stevens,

743 M.H.H., & Wagner, H., 2008. The vegan package. Community Ecol. Packag. 190.

744 Paulson, J.N., Colin Stine, O., Bravo, H.C., Pop, M., 2013. Differential abundance analysis
745 for microbial marker-gene surveys. Nat. Methods 10, 1200–1202.
746 https://doi.org/10.1038/nmeth.2658

747 Ponette-González, A.G., Van Stan, J.T., Magyar, D., 2020. Things seen and unseen in
748 throughfall and stemflow, in: Precipitation Partitioning by Vegetation: A Global
749 Synthesis. Springer, Cham, pp. 70–87. https://doi.org/10.1007/978-3-030-29702-2_5

750 Potthast, K., Meyer, S., Crecelius, A.C., Schubert, U.S., Tischer, A., Michalzik, B., 2017.
751 Land-use and fire drive temporal patterns of soil solution chemistry and nutrient fluxes.
752 Sci. Total Environ. 605–606, 514–526.
753 https://doi.org/10.1016/J.SCITOTENV.2017.06.182

754 Quast, C., Pruesse, E., Yilmaz, P., Gerken, J., Schweer, T., Yarza, P., Peplies, J., Glöckner,
755 F.O., 2013. The SILVA ribosomal RNA gene database project: improved data
756 processing and web-based tools. Nucleic Acids Res. 41, 590–596.
757 https://doi.org/10.1093/nar/gks1219

758 Reche, I., D'Orta, G., Mladenov, N., Winget, D.M., Suttle, C.A., 2018. Deposition rates of
759 viruses and bacteria above the atmospheric boundary layer. ISME J. 12, 1154–1162.
760 https://doi.org/10.1038/s41396-017-0042-4

761 Rolando, J.L., Kolton, M., Song, T., Kostka, J.E., 2022. The core root microbiome of Spartina
762 alterniflora is predominated by sulfur-oxidizing and sulfate-reducing bacteria in Georgia
763 salt marshes, USA. Microbiome 10. https://doi.org/10.1186/s40168-021-01187-7

764 Sadeghi, S.M.M., Gordon, D.A., Van Stan, J.T., 2020. A global synthesis of throughfall and
765 stemflow hydrometeorology, in: Precipitation Partitioning by Vegetation: A Global
766 Synthesis. Springer International Publishing, pp. 48–69. https://doi.org/10.1007/978-3-
767 030-29702-2_4

768 Sánchez-Parra, B., Núñez, A., García, A.M., Campoy, P., Moreno, D.A., 2021. Distribution of
769 airborne pollen, fungi and bacteria at four altitudes using high-throughput DNA
770 sequencing. Atmos. Res. 249, 105306. https://doi.org/10.1016/j.atmosres.2020.105306

771 Scheiner, D., 1974. A modified version of the sodium salicylate method for analysis of
772 wastewater nitrates. Water Res. 8, 835–840. https://doi.org/10.1016/0043-
773 1354(74)90030-X

774 Schliep, K.P., 2011. phangorn: Phylogenetic analysis in R. Bioinformatics 27, 592–593.
775 https://doi.org/10.1093/bioinformatics/btq706

776 Seelmeyer, G., 1954. Deutsche Einheitsverfahren zur Wasseruntersuchung.
777 Herausgegeben im Auftrage der Fachgruppe Wasserchemie in der Gesellschaft
778 Deutscher Chemiker E. V. Bearbeitet von L. W. Haase, H. Stooff, G. Gad, W. Wesly
779 u.a. Verlag Chemie, Weinheim/Bergstraße 1954, 180. Mater. Corros. 5, 357–357.
780 https://doi.org/10.1002/maco.19540050819

781 Stoddard, S.F., Smith, B.J., Hein, R., Roller, B.R.K., Schmidt, T.M., 2015. rrnDB: Improved
782 tools for interpreting rRNA gene abundance in bacteria and archaea and a new
783 foundation for future development. Nucleic Acids Res. 43, 593–598.
784 https://doi.org/10.1093/nar/gku1201

785 Takai, K., Horikoshi, K., 2000. Rapid detection and quantification of members of the archaeal
786 community by quantitative PCR using fluorogenic probes. Appl. Environ. Microbiol. 66,
787 5066–5072. https://doi.org/10.1128/AEM.66.11.5066-5072.2000

788 Teachey, M.E., Pound, P., Ottesen, E.A., Van Stan, J.T., 2018. Bacterial community

composition of throughfall and stemflow. Front. For. Glob. Chang. 1. https://doi.org/10.3389/ffgc.2018.00007

Team, R.C., 2020. A Language and Environment for Statistical Computing. R Found. Stat. Comput.

Tischer, A., Michalzik, B., Lotze, R., 2020. Nonuniform but highly preferential stemflow routing along bark surfaces and actual smaller infiltration areas than previously assumed: A case study on European beech (Fagus sylvatica L.) and sycamore maple (Acer pseudoplatanus L.). Ecohydrology 13, e2230. https://doi.org/10.1002/eco.2230

Vacher, C., Hampe, A., Porté, A.J., Sauer, U., Compant, S., Morris, C.E., 2016. The Phyllosphere: Microbial Jungle at the Plant-Climate Interface. Annu. Rev. Ecol. Evol. Syst. 47, 1–24. https://doi.org/10.1146/annurev-ecolsys-121415-032238

Van Stan, J.T., Morris, C.E., Aung, K., Kuzyakov, Y., Magyar, D., Rebollar, E.A., Remus-Emsermann, M., Uroz, S., Vandenkoornhuyse, P., 2020. Precipitation partitioning—hydrologic highways between microbial communities of the plant microbiome?, in: Precipitation Partitioning by Vegetation: A Global Synthesis. Springer International Publishing, pp. 228–251. https://doi.org/10.1007/978-3-030-29702-2_14

Van Stan, J.T., Ponette-González, A.G., Swanson, T., Weathers, K.C., 2021. Throughfall and stemflow are major hydrologic highways for particulate traffic through tree canopies. Front. Ecol. Environ. 19, 404–410. https://doi.org/10.1002/fee.2360

Van Stan, J.T., Stubbins, A., 2018. Tree-DOM: Dissolved organic matter in throughfall and stemflow. Limnol. Oceanogr. Lett. 3, 199–214. https://doi.org/10.1002/lol2.10059

Van Stan, J.T., Wagner, S., Guillemette, F., Whitetree, A., Lewis, J., Silva, L., Stubbins, A., 2017. Temporal Dynamics in the Concentration, Flux, and Optical Properties of Tree-Derived Dissolved Organic Matter in an Epiphyte-Laden Oak-Cedar Forest. J. Geophys. Res. Biogeosciences 122, 2982–2997. https://doi.org/10.1002/2017JG004111

Visco, G., Campanella, L., Nobili, V., 2005. Organic carbons and TOC in waters: An overview of the international norm for its measurements, in: Microchemical Journal. Elsevier, 79, pp. 185–191. https://doi.org/10.1016/j.microc.2004.10.018

Vorholt, J.A., 2012. Microbial life in the phyllosphere. Nat. Rev. Microbiol. 10, 828-840. https://doi.org/10.1038/nrmicro2910

Vrede, K., Heldal, M., Norland, S., Bratbak, G., 2002. Elemental composition (C, N, P) and cell volume of exponentially growing and nutrient-limited bacterioplankton. Appl. Environ. Microbiol. 68, 2965–2971. https://doi.org/10.1128/AEM.68.6.2965-2971.2002

Wickham, H., Averick, M., Bryan, J., Chang, W., McGowan, L., François, R., Grolemund, G., Hayes, A., Henry, L., Hester, J., Kuhn, M., Pedersen, T., Miller, E., Bache, S., Müller, K., Ooms, J., Robinson, D., Seidel, D., Spinu, V., Takahashi, K., Vaughan, D., Wilke, C., Woo, K., Yutani, H., 2019. Welcome to the Tidyverse. J. Open Source Softw. 4, 1686. https://doi.org/10.21105/joss.01686

Williams, C.G., 2013. Forest tree pollen dispersal via the water. Am. J. Bot. 100, 1184–1190. https://doi.org/10.3732/ajb.1300085

Wright, E.S., 2020. RNAcontest: Comparing tools for noncoding RNA multiple sequence alignment based on structural consistency. RNA 26, 531–540. https://doi.org/10.1261/rna.073015.119

Wright, E.S., 2016. Using DECIPHER v2.0 to analyze big biological sequence data in R. R J. 8, 352–359. https://doi.org/10.32614/rj-2016-025

Xu, S., Li, L., Luo, X., Chen, M., Tang, W., Zhan, L., Dai, Z., Lam, T.T., Guan, Y., Yu, G., 2022. Ggtree: A serialized data object for visualization of a phylogenetic tree and annotation data. iMeta 1, 56. https://doi.org/10.1002/imt2.56

Xu, S., Zhan, L., Tang, W., Wang, Q., Dai, Z., Zhou, L., Feng, T., Chen, M., Wu, T., Hu, E., Yu, G., 2023. MicrobiotaProcess: A comprehensive R package for deep mining microbiome. Innovation 4, 100388. https://doi.org/10.1016/j.xinn.2023.100388

Zhang, L., Lehmann, K., Totsche, K.U., Lueders, T., 2018. Selective successional transport of bacterial populations from rooted agricultural topsoil to deeper layers upon extreme precipitation events. Soil Biol. Biochem. 124, 168–178. https://doi.org/10.1016/j.soilbio.2018.06.012

Figures

848 Figure 1: Study site and study design for sample collection at the Hainich Critical Zone Exploratory in western
849 Thuringia, Germany. A) Sampling was conducted at an open area-site for rainwater representative of
850 above-canopy precipitation and at a mixed beech forest site for phyllosphere, throughfall, stemflow, and
851 seepage and soil sampling at different depths. B) Number of samples for each sample type across two
852 sampling time points. C) Conceptional representation of samples spanning from the tree canopy down to
853 the soil, and photographs of the two tree species, sample collectors and a typical soil core.
854 Figure 2: Bacterial transport across the different compartments, and contributions and correlations to
855 transported carbon and nitrogen. A) Fluxes of TOC and TN expressed per m^2, bacterial contributions to
856 TOC and TN content, and fluxes of bacterial cells per m^2 across the different compartments during an
857 early and late growing season rain event. Each symbol represents a single sample, and the crossbar
858 depicts the average for each sample type. Significant differences are shown in letter code tested by post
859 hoc Dunn's multiple comparing ($p < 0.05$). B) Spearman's rank correlation (r_s) between estimated
860 bacterial cell numbers and TOC and TN of water samples per sampling event in May and September.
861 Figure 3: Bacterial communities across rainwater (n = 8), leaves (n = 48), throughfall (n = 20), stemflow (n = 8),
862 seepage (n = 25) and soil (n = 34) samples. A) Observed ASV richness (left panel) and Shannon index (right
863 panel). Single data points are shown as dots for samples from May and triangles from September
864 (crossbar represents mean of values). Letter code indicates significant differences between types and
865 indexes after Dunn's post hoc test ($p < 0.05$). B) Distribution of most abundant bacterial families depicted
866 as NMDS based on Bray-Curtis dissimilarities across all samples. Results of PERMANOVA (9999
867 permutations) are displayed as Venn diagram, asterisks depict confidence interval at $p < 0.001$ for each
868 accounting factor. C) Bacterial community composition of most abundant bacterial families with more
869 than 1 % absolute read abundance per event. Single stacked bars show the relative read abundance of
870 16S rRNA gene sequences on family level.
871 Figure 4: Prediction of metabolic functions of bacterial communities across the different sample types and the
872 two time points. A) Abundance of KEGG orthologues (KO) corresponding to genes for enzymes of
873 selected metabolic pathways. The size of the bubbles depicts the mean relative KO abundance of each
874 sample type. B) Proportions of bacterial communities employing the predicted KO. Small dots depict the
875 mean relative abundance of bacterial classes per sample and the bigger dots represent the mean relative

abundance for a given sample type. Letter code displays significant differences between sample types within each pathway based on post hoc Dunn's multiple comparing ($p < 0.05$).

Figure 5: Phylogeny and relative abundance of bacterial core taxa across rainwater, phyllosphere, throughfall, stemflow and seepage samples during both sampling time points. The tree is based on a neighbor-joining model of a 16S rRNA gene alignment. The color and shape of each node show the presence of an ASV on family-level and on genus-level, respectively, at a given sample type. The size of nodes depicts the mean relative abundance of each ASV across the sample types. Stacked bars display the mean relative abundance of each ASV across all samples from both sampling points of rain, phyllosphere, throughfall, stemflow and seepage communities.

Figure 1

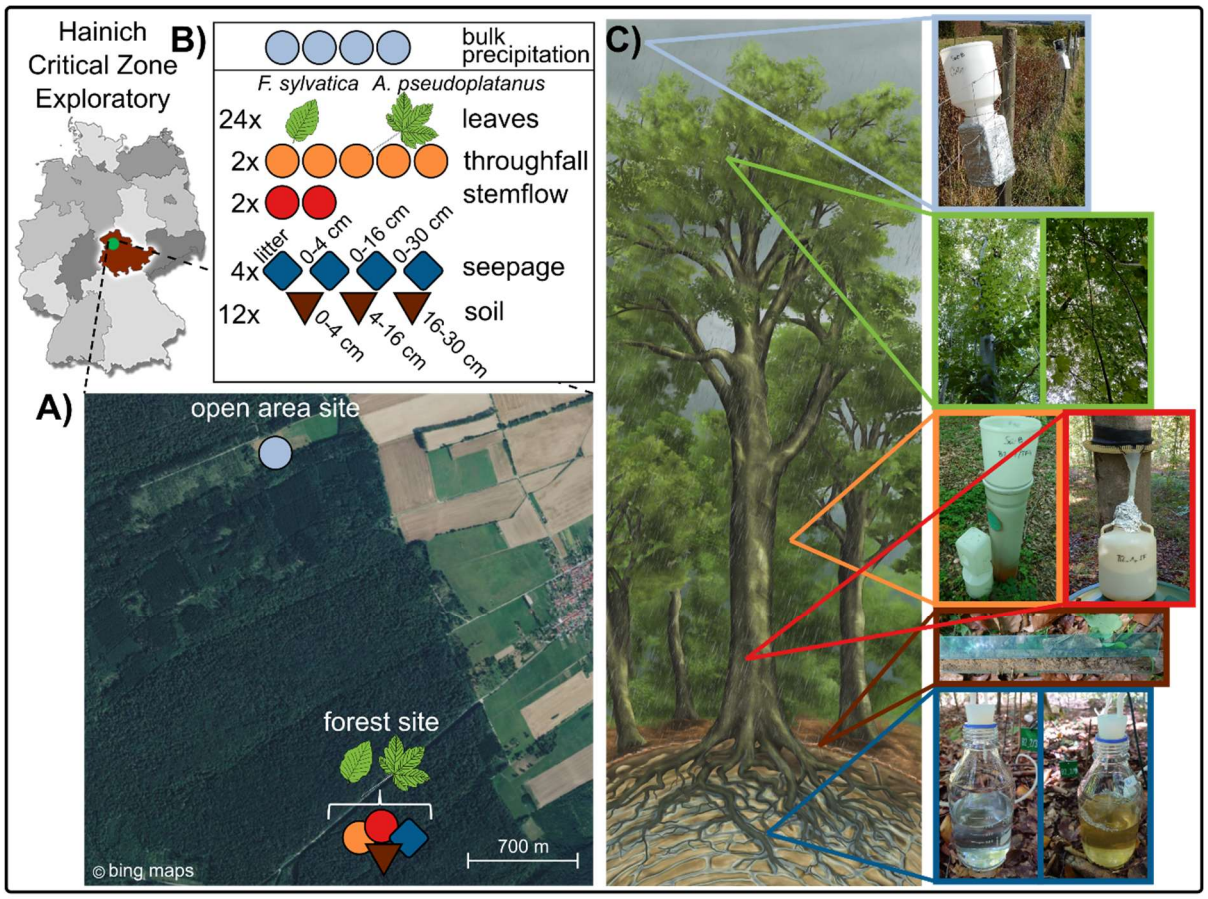

Figure 1: Study site and study design for sample collection at the Hainich Critical Zone Exploratory in western Thuringia, Germany. **A)** Sampling was conducted at an open area-site for rainwater representative of above-canopy precipitation and at a mixed beech forest site for phyllosphere, throughfall, stemflow, and seepage and soil sampling at different depths. **B)** Number of samples for each sample type across two sampling time points. **C)** Conceptional representation of samples spanning from the tree canopy down to the soil, and photographs of the two tree species, sample collectors and a typical soil core.

Figure 2

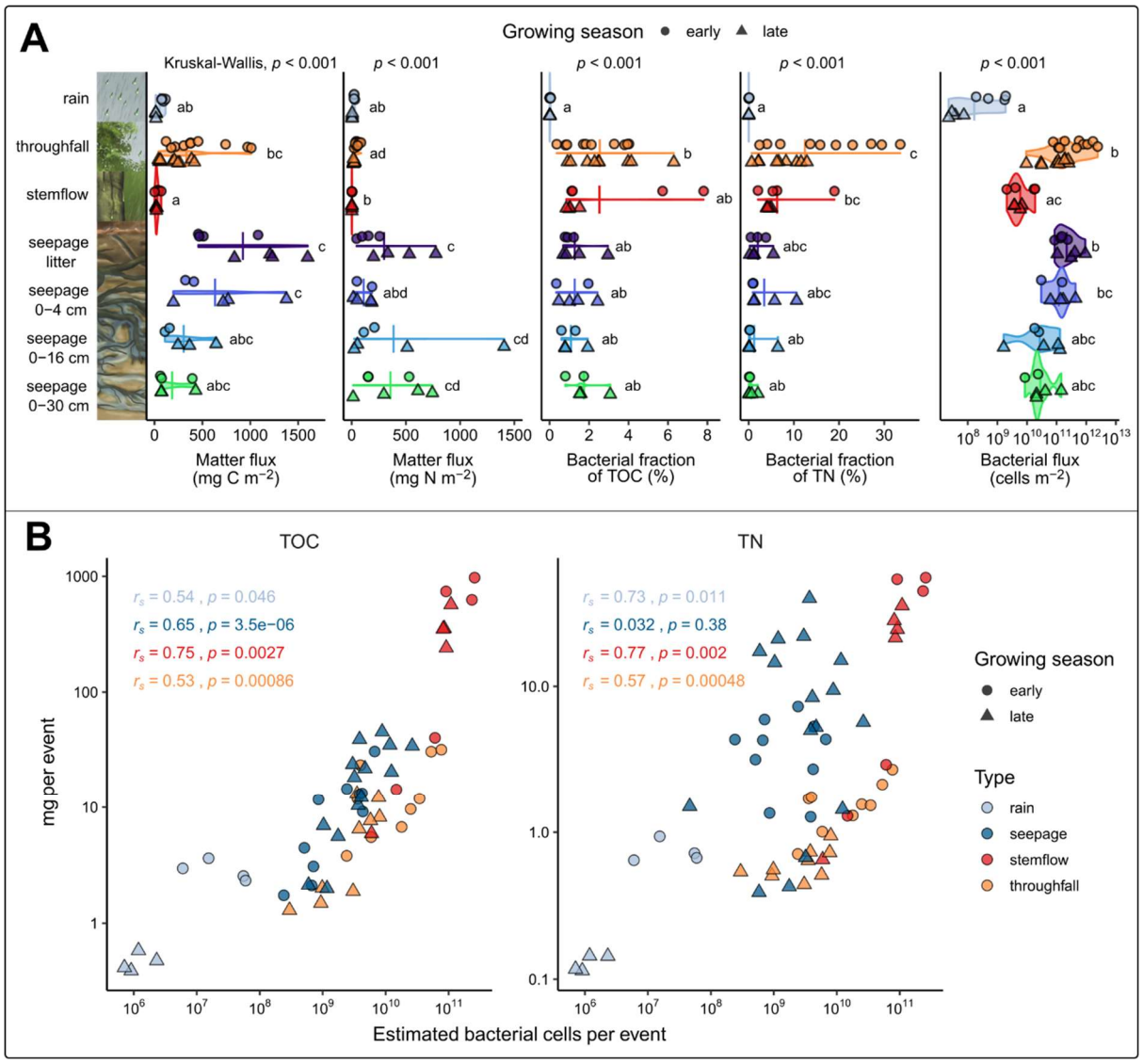

Figure 2: Bacterial transport across the different compartments, and contributions and correlations to transported carbon and nitrogen. **A)** Fluxes of TOC and TN expressed per m^2, bacterial contributions to TOC and TN content, and fluxes of bacterial cells per m^2 across the different compartments during an early and late growing season rain event. Each symbol represents a single sample, and the crossbar depicts the average for each sample type. Significant differences are shown in letter code tested by post hoc Dunn's multiple comparing ($p < 0.05$). **B)** Spearman's rank correlation (r_s) between estimated bacterial cell numbers and TOC and TN of water samples per sampling event in May and September.

905 **Figure 3**

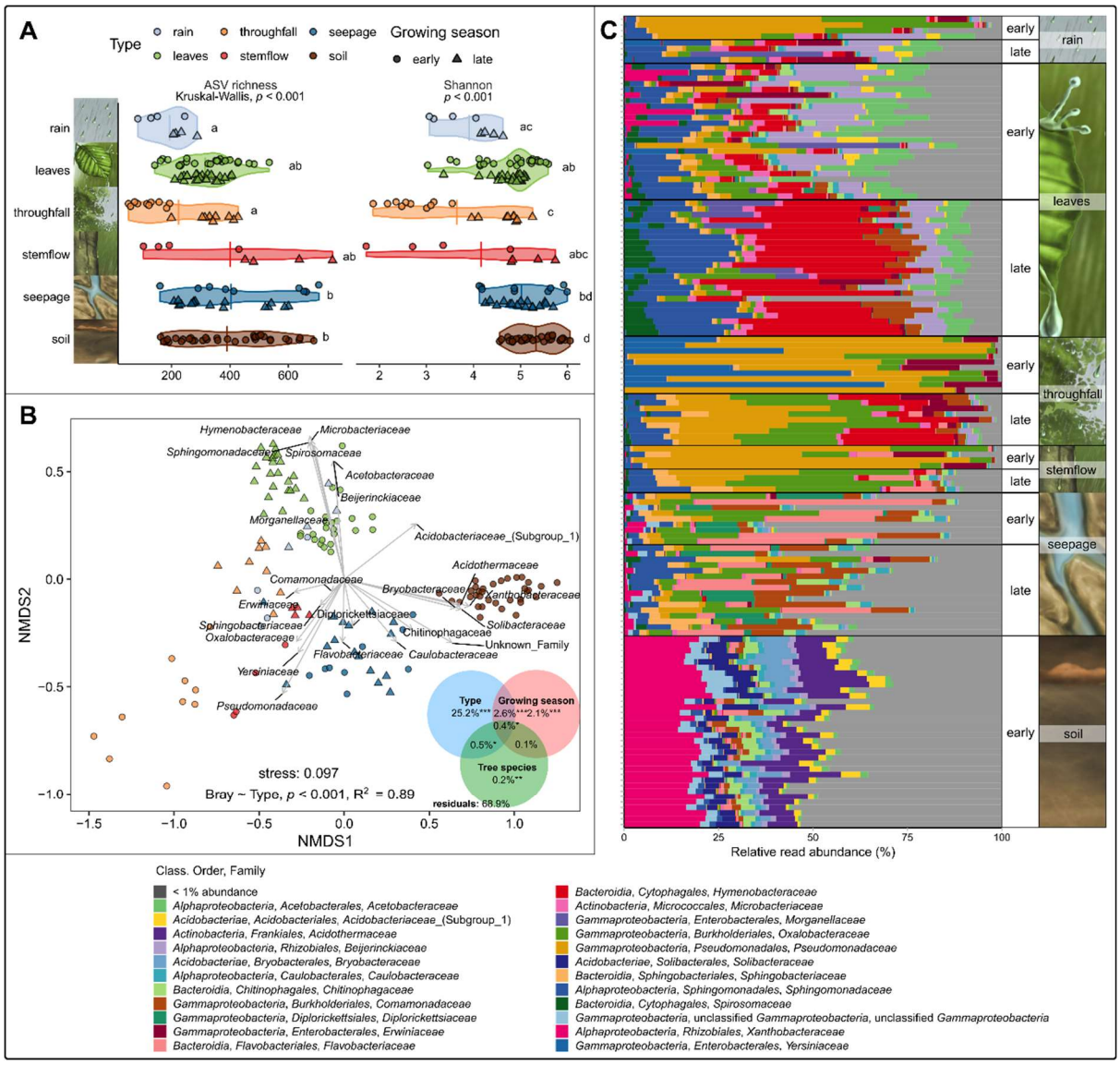

906

907 **Figure 3:** Bacterial communities across rainwater (n = 8), leaves (n = 48), throughfall (n = 20), stemflow
908 (n = 8), seepage (n = 25) and soil (n = 34) samples. **A)** Observed ASV richness (left panel) and Shannon
909 index (right panel). Single data points are shown as dots for samples from May and triangles from
910 September (crossbar represents mean of values). Letter code indicates significant differences between
911 types and indexes after Dunn's post hoc test ($p < 0.05$). **B)** Distribution of most abundant bacterial
912 families depicted as NMDS based on Bray-Curtis dissimilarities across all samples. Results of
913 PERMANOVA (9999 permutations) are displayed as Venn diagram, asterisks depict confidence interval
914 at $p < 0.001$ for each accounting factor. **C)** Bacterial community composition of most abundant bacterial
915 families with more than 1 % absolute read abundance per event. Single stacked bars show the relative
916 read abundance of 16S rRNA gene sequences on family level.

Figure 4

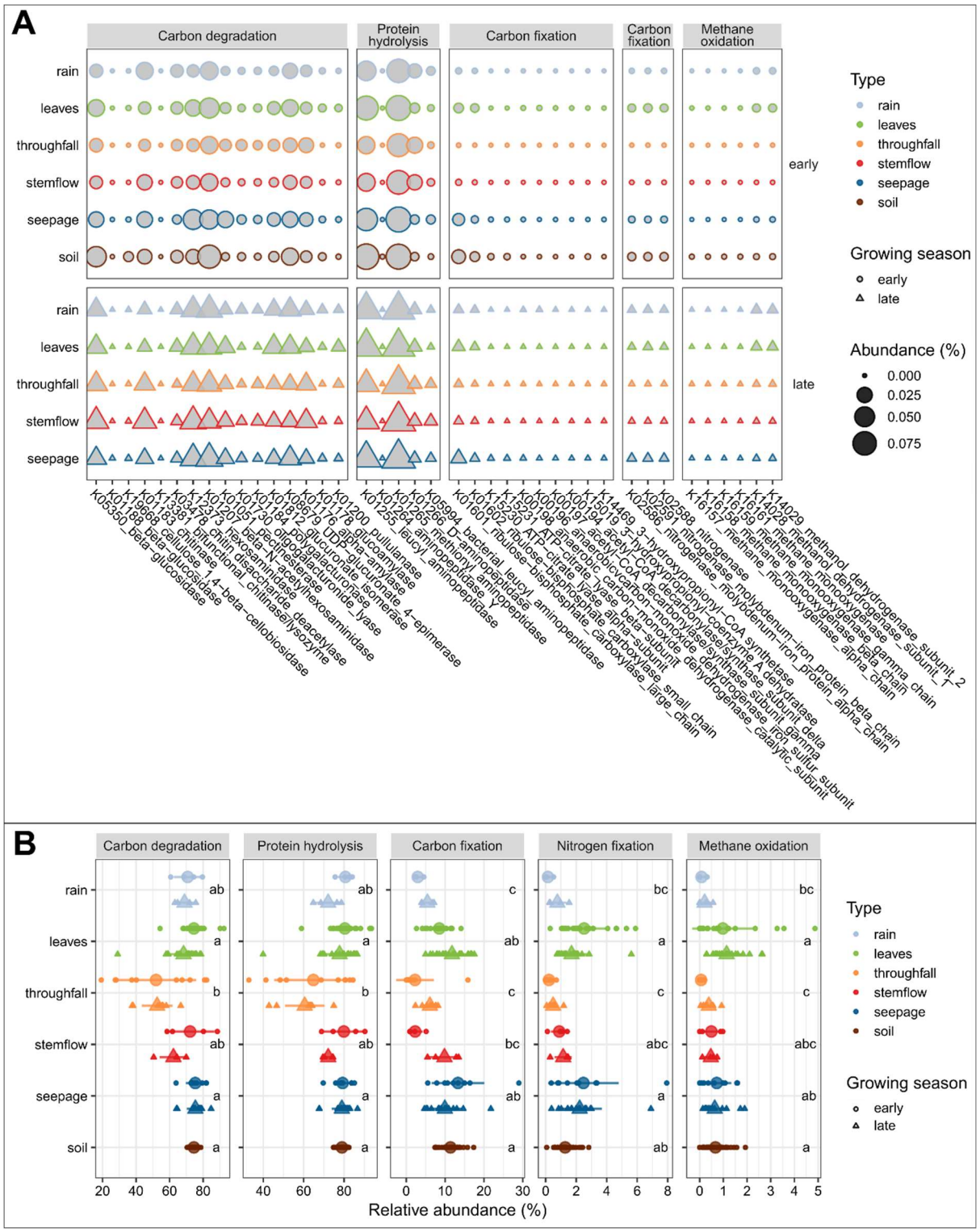

Figure 4: Prediction of metabolic functions of bacterial communities across the different sample types and the two time points. **A)** Abundance of KEGG orthologues (KO) corresponding to genes for enzymes of selected metabolic pathways. The size of the bubbles depicts the mean relative KO abundance of each sample type. **B)** Proportions of bacterial communities employing the predicted KO. Small dots depict the mean relative abundance of bacterial classes per sample and the bigger dots represent the mean relative abundance for a given sample type. Letter code displays significant differences between sample types within each pathway based on post hoc Dunn's multiple comparing ($p < 0.05$).

Figure 5

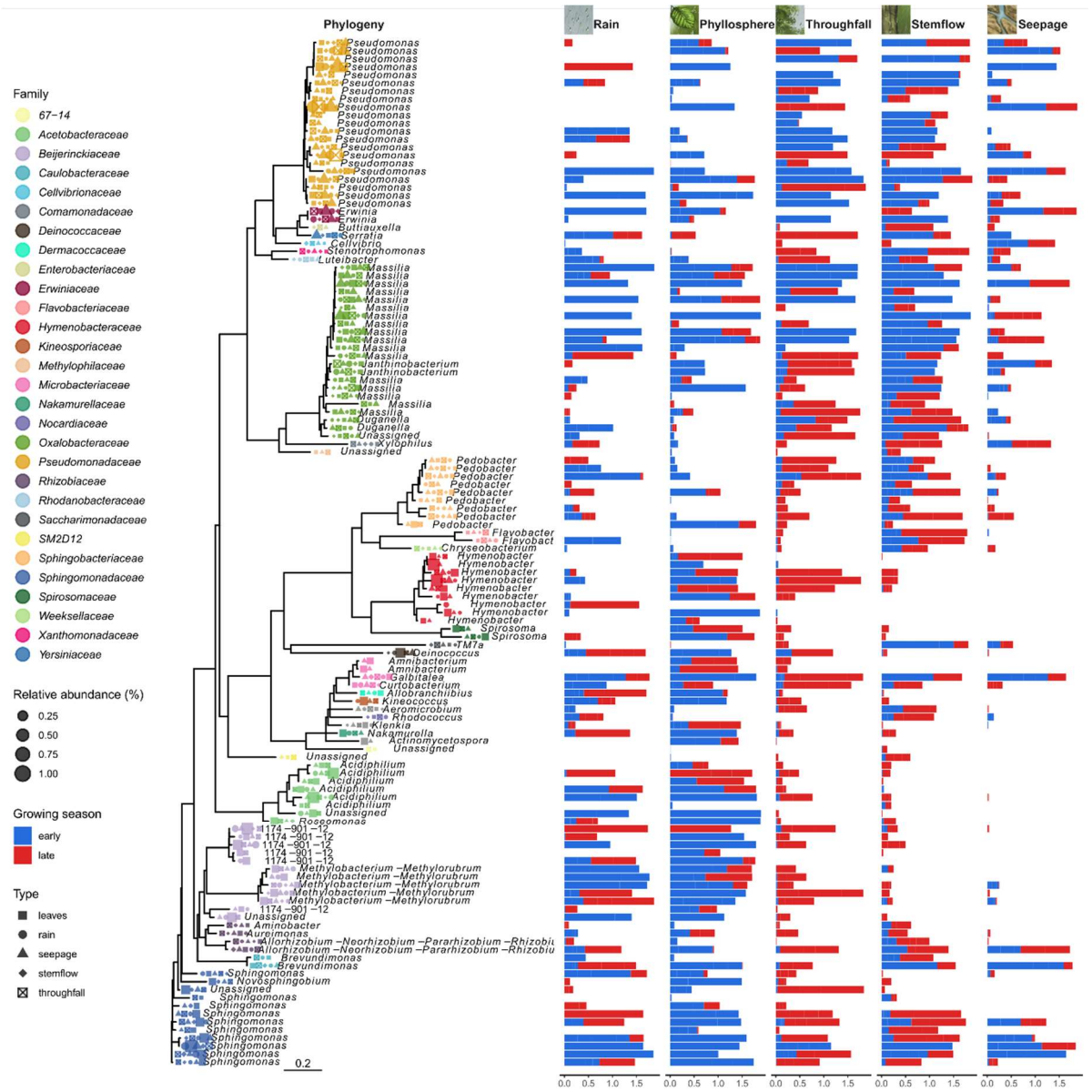

Figure 5: Phylogeny and relative abundance of bacterial core taxa across rainwater, phyllosphere, throughfall, stemflow and seepage samples during both sampling time points. The tree is based on a neighbor-joining model of a 16S rRNA gene alignment. The color and shape of each node show the presence of an ASV on family-level and on genus-level, respectively, at a given sample type. The size of nodes depicts the mean relative abundance of each ASV across the sample types. Stacked bars display the mean relative abundance of each ASV across all samples from both sampling points of rain, phyllosphere, throughfall, stemflow and seepage communities.

935

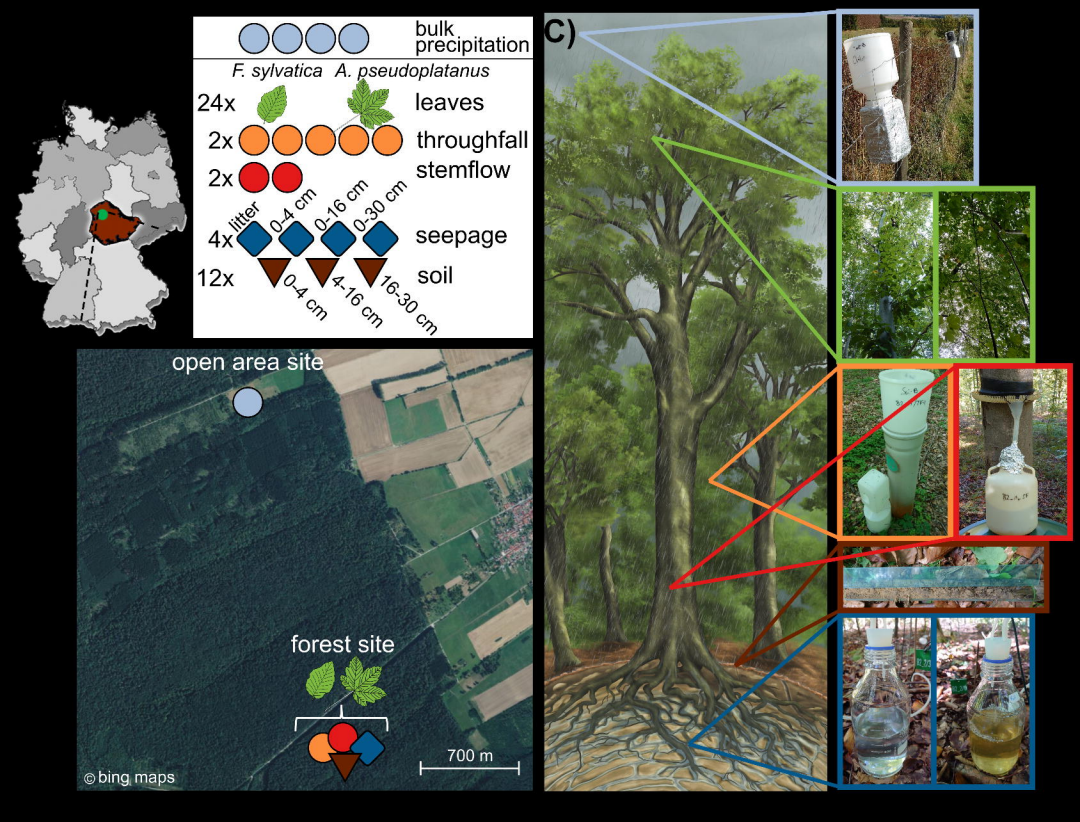
bulk precipitation
F. sylvatica
A. pseudoplatanus
24x
leaves
2x
throughfall
2x
stemflow
litter
0-4 cm
0-16 cm
0-30 cm
4x
seepage
12x
0-4 cm
4-16 cm
16-30 cm
soil
open area site
forest site
700 m
© bing maps
C)

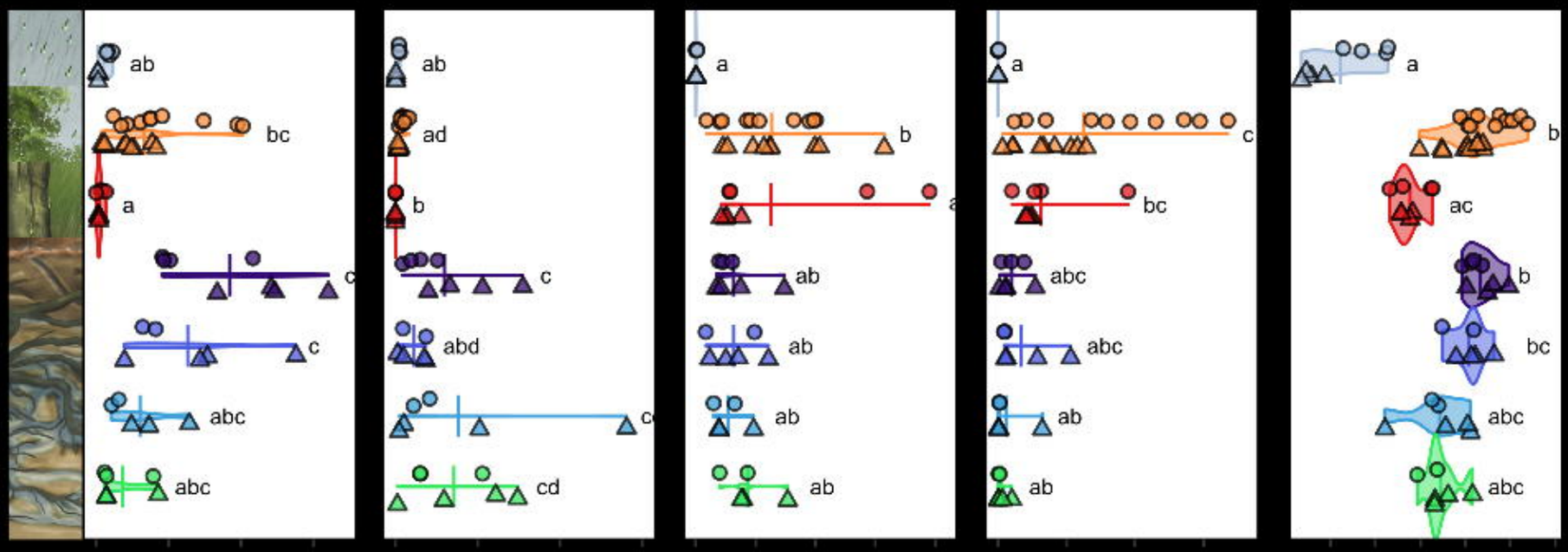
ab
bc
a
c
c
abc
abc
ab
ad
b
c
abd
c
cd
a
b
a
ab
ab
ab
ab
a
c
bc
abc
abc
ab
ab
a
b
ac
b
bc
abc
abc

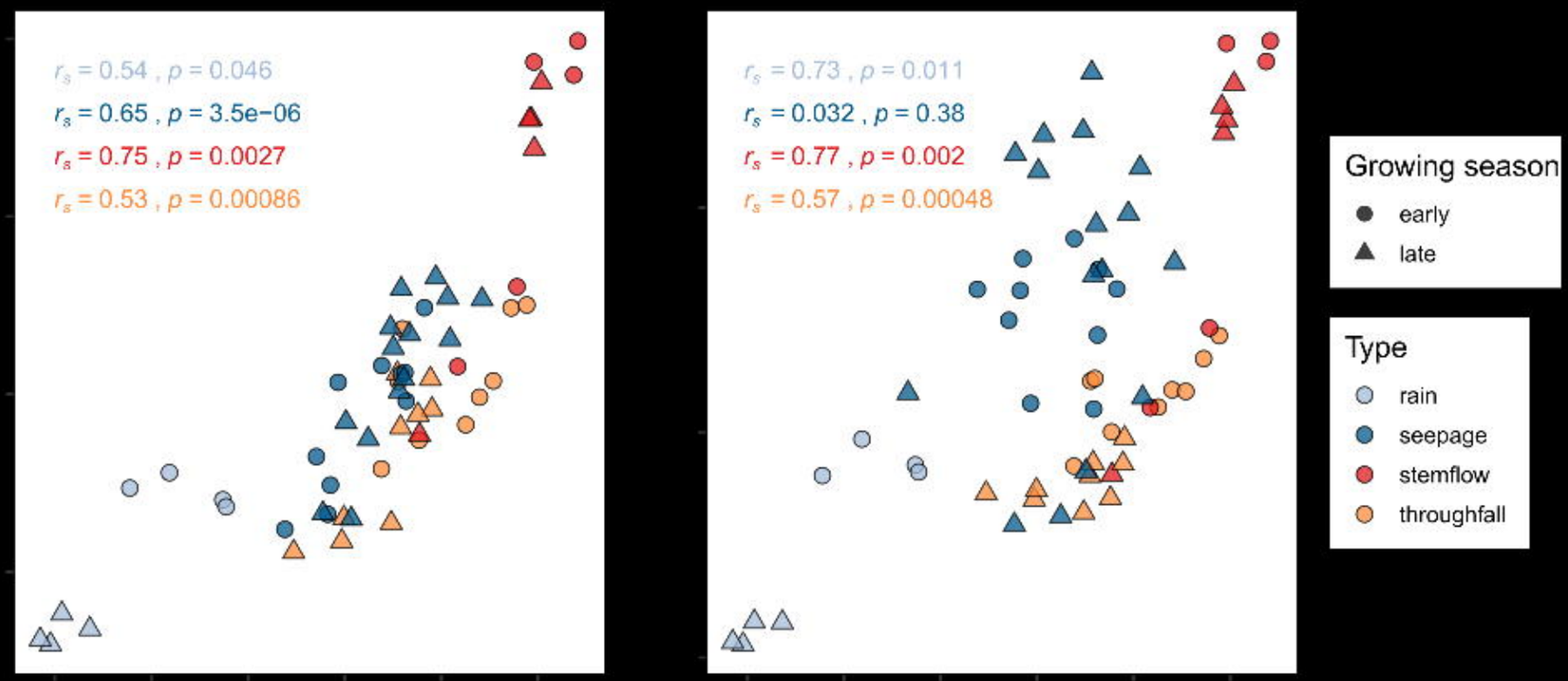
TOC
r_s = 0.54 , p = 0.046
r_s = 0.65 , p = 3.5e−06
r_s = 0.75 , p = 0.0027
r_s = 0.53 , p = 0.00086
TN
r_s = 0.73 , p = 0.011
r_s = 0.032 , p = 0.38
r_s = 0.77 , p = 0.002
r_s = 0.57 , p = 0.00048
Growing season
early
late
Type
rain
seepage
stemflow
throughfall

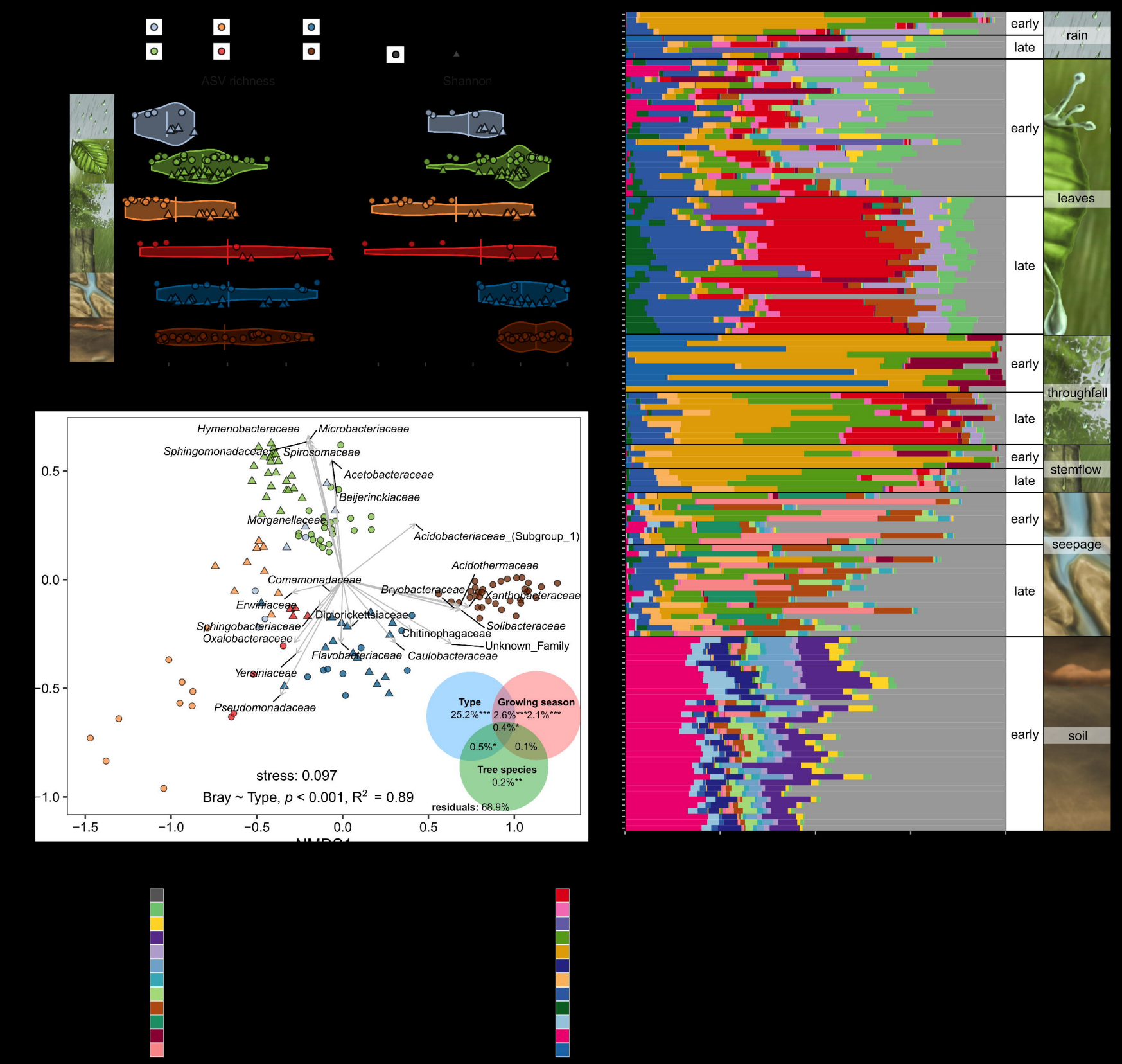
ASV richness
Shannon
Hymenobacteraceae
Microbacteriaceae
Sphingomonadaceae
Spirosomaceae
Acetobacteraceae
Beijerinckiaceae
Morganellaceae
Acidobacteriaceae_(Subgroup_1)
Acidothermaceae
Comamonadaceae
Bryobacteraceae
Xanthobacteraceae
Erwiniaceae
Diplorickettsiaceae
Sphingobacteriaceae
Solibacteraceae
Oxalobacteraceae
Chitinophagaceae
Unknown_Family
Flavobacteriaceae
Caulobacteraceae
Yersiniaceae
Pseudomonadaceae
Type
25.2%***
Growing season
2.6%***
2.1%***
0.4%*
0.5%*
0.1%
Tree species
0.2%**
residuals: 68.9%
stress: 0.097
Bray ~ Type, p < 0.001, R2 = 0.89
0.5
0.0
−0.5
−1.0
−1.5
−1.0
−0.5
0.0
0.5
1.0
early
late
rain
leaves
throughfall
stemflow
seepage
soil

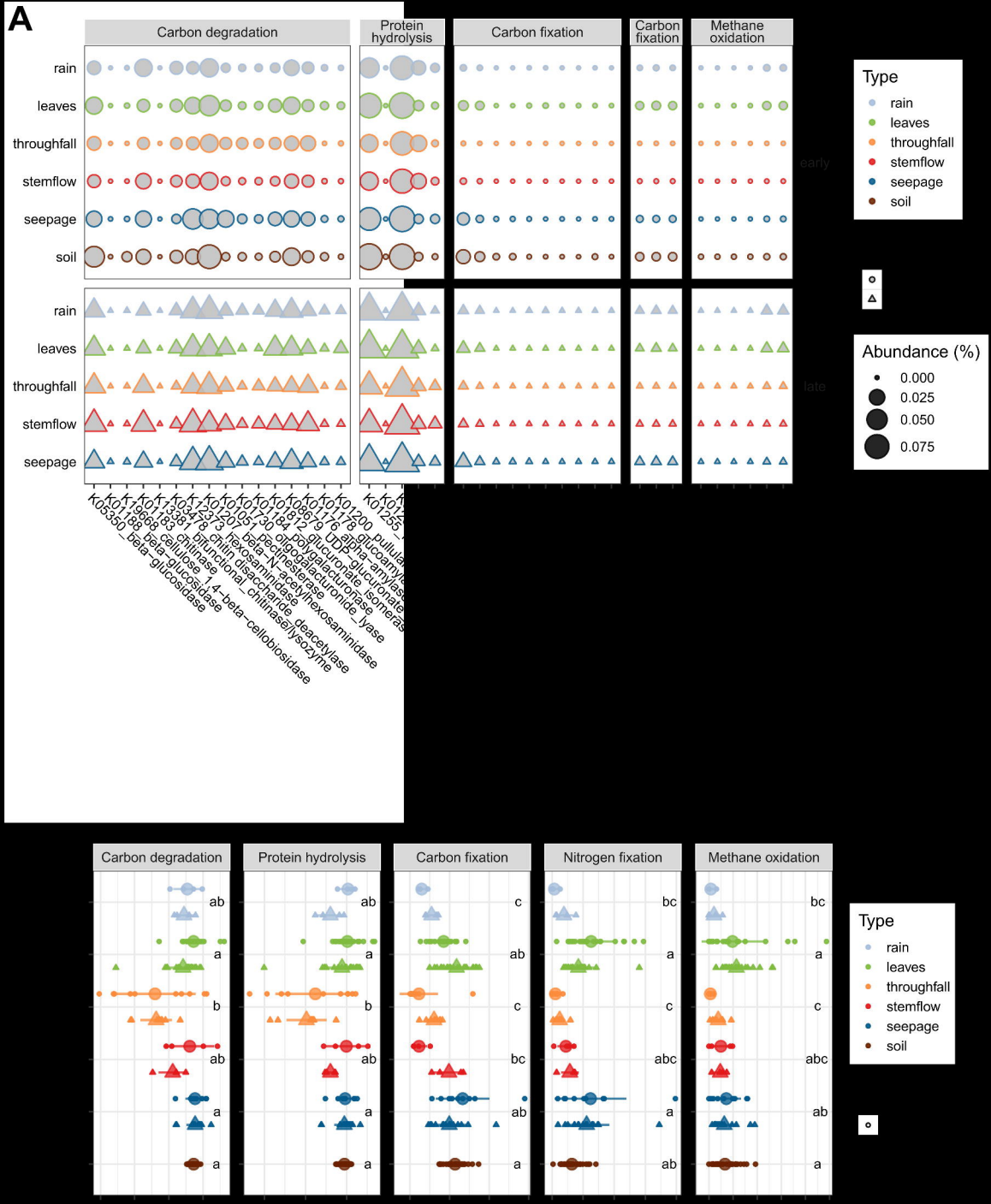
A
Carbon degradation
Protein hydrolysis
Carbon fixation
Carbon fixation
Methane oxidation
rain
leaves
throughfall
stemflow
seepage
soil
early
late
Type
rain
leaves
throughfall
stemflow
seepage
soil
Abundance (%)
0.000
0.025
0.050
0.075
K05350_beta-glucosidase
K01188_beta-glucosidase
K19668_cellulose 1,4-beta-cellobiosidase
K01183_chitinase
K13381_bifunctional_chitinase/lysozyme
K03478_chitin disaccharide deacetylase
K12373_hexosaminidase
K01207_beta-N-acetylhexosaminidase
K01051_pectinesterase
K01730_oligogalacturonide_lyase
K01184_polygalacturonase
K01812_glucuronate isomerase
K08679_UDP-glucuronate
K01176_alpha-amylase
K01178_glucoamylase
K01200_pullulan
Carbon degradation
Protein hydrolysis
Carbon fixation
Nitrogen fixation
Methane oxidation
ab
a
b
ab
a
a
ab
a
b
ab
a
a
c
ab
c
bc
ab
a
bc
a
c
abc
a
ab
bc
a
c
abc
ab
a
Type
rain
leaves
throughfall
stemflow
seepage
soil

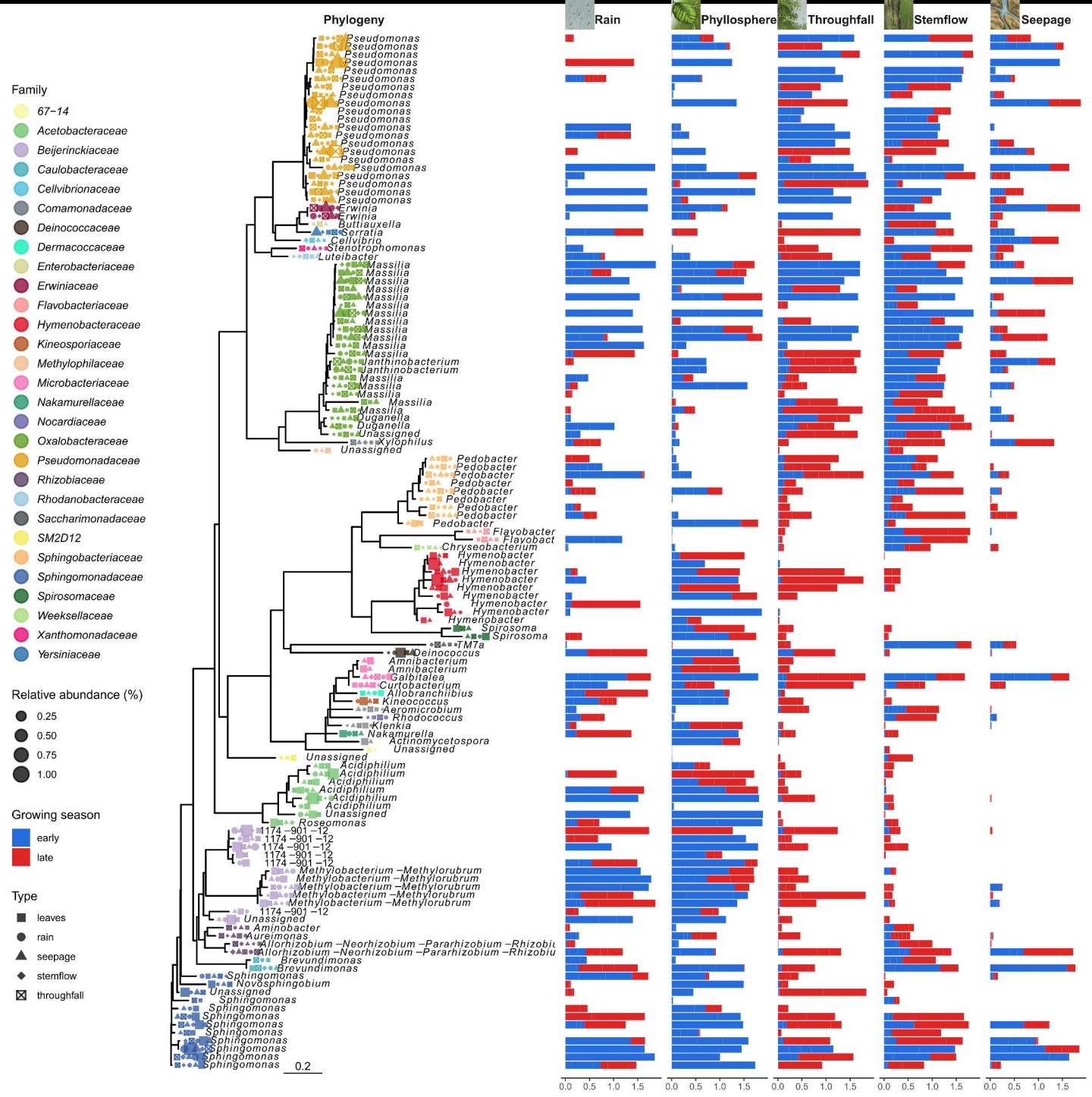
Phylogeny
Rain
Phyllosphere
Throughfall
Stemflow
Seepage
Family
67−14
Acetobacteraceae
Beijerinckiaceae
Caulobacteraceae
Cellvibrionaceae
Comamonadaceae
Deinococcaceae
Dermacoccaceae
Enterobacteriaceae
Erwiniaceae
Flavobacteriaceae
Hymenobacteraceae
Kineosporiaceae
Methylophilaceae
Microbacteriaceae
Nakamurellaceae
Nocardiaceae
Oxalobacteraceae
Pseudomonadaceae
Rhizobiaceae
Rhodanobacteraceae
Saccharimonadaceae
SM2D12
Sphingobacteriaceae
Sphingomonadaceae
Spirosomaceae
Weeksellaceae
Xanthomonadaceae
Yersiniaceae
Relative abundance (%)
0.25
0.50
0.75
1.00
Growing season
early
late
Type
leaves
rain
seepage
stemflow
throughfall
Pseudomonas
Erwinia
Buttiauxella
Serratia
Cellvibrio
Stenotrophomonas
Luteibacter
Massilia
Xanthinobacterium
Duganella
Unassigned
Xylophilus
Pedobacter
Flavobacter
Chryseobacterium
Hymenobacter
Spirosoma
TM7a
Deinococcus
Amnibacterium
Gaiella
Curtobacterium
Allobranchiibius
Kineococcus
Aureimicrobium
Rhodococcus
Klenkia
Nakamurella
Actinomycetospora
Acidiphilium
Roseomonas
1174−901−12
Methylobacterium−Methylorubrum
Aminobacter
Aureimonas
Allorhizobium−Neorhizobium−Pararhizobium−Rhizobiu
Brevundimonas
Sphingomonas
Novosphingobium
0.2
0.0
0.5
1.0
1.5